PLASMA-PROPELLANT INTERACTIONS

Final Report
by

Dr W G Proud, P Kalafatis, Dr M J Gifford, Dr M W Greenaway,
C Dobson and Professor J E Field
October 2003

9109-CH-01

Research for US Navy, ONRRO, Boston, USA

Reports sent to: USARDGG-UK
Edison House
223 Old Marylebone Road
London
NW1 5TH
UK

CONTRACT NUMBER N68171-01-C-9016

PCS
University of Cambridge
Department of Physics
Cavendish Laboratory
Madingley Road
Cambridge
CB3 0HE
UK

REPORT DOCUMENTATION PAGE

Form Approved
OMB No. 0704-0188

1. AGENCY USE ONLY *(Leave blank)*	2. REPORT DATE	3. REPORT TYPE AND DATES COVERED
	3 FEB 04	FINAL REPORT OCTOBER 2003

4. TITLE AND SUBTITLE
PLASMA-PROPELLANT INTERACTIONS

5. FUNDING NUMBERS
9109-CH-01
N68171-01-C-9016

6. AUTHOR(S)
DR. W.G. PROUD, P. KALAFATIS, DR. M.J. GIFFORD. DR. M.W. GREENAWAY, C. DOBSON, PROFESSOR J.E. FIELD

7. PERFORMING ORGANIZATION NAME(S) AND ADDRESS(ES)
UNIVERSITY OF CAMBRIDGE
DEPARTMENT OF PHYSICS
CAVENDISH LABORATORY
MADINGLEY ROAD
CAMBRIDGE CB3 0HE, UK

8. PERFORMING ORGANIZATION REPORT NUMBER
RG 32402

9. SPONSORING / MONITORING AGENCY NAME(S) AND ADDRESS(ES)
U.S. ARMY - EUROPEAN RESEARCH OFFICE
EDISON HOUSE
223 OLD MARYLEBONE ROAD
LONDON NW1 5TH
UNITED KINGDOM

10. SPONSORING / MONITORING AGENCY REPORT NUMBER

11. SUPPLEMENTARY NOTES

12a. DISTRIBUTION / AVAILABILITY STATEMENT
APPROVED FOR PUBLIC RELEASE
DISTRIBUTION UNLIMITED
FINAL REPORT

12b. DISTRIBUTION CODE

13. ABSTRACT *(Maximum 200 words)*

14. SUBJECT TERMS
PLASMA, PROPELLANT, EXPLOSIVES, DEFLAGRATION TO DETONATION TRANSITION, MICROSCOPY

15. NUMBER OF PAGES
45

16. PRICE CODE

17. SECURITY CLASSIFICATION OF REPORT	18. SECURITY CLASSIFICATION OF THIS PAGE	19. SECURITY CLASSIFICATION OF ABSTRACT	20. LIMITATION OF ABSTRACT
UNCLASSIFIED	UNCLASSIFIED	UNCLASSIFIED	UL

REPORT DOCUMENTATION PAGE

Form Approved
OMB No. 074-0188

1. AGENCY USE ONLY (Leave blank)	2. REPORT DATE	3. REPORT TYPE AND DATES COVERED
	October 2003	Final Report

4. TITLE AND SUBTITLE

Propellant-Plasma Interactions

5. FUNDING NUMBERS

6. AUTHOR(S)

Dr W G Proud, P Kalafatis, Dr M J Gifford,
Dr M W Greenaway, C Dobson, Professor J E Field

7. PERFORMING ORGANIZATION NAME(S) AND ADDRESS(ES)

University of Cambridge
Department of Physics, Cavendish Laboratory,
Madingley Road, Cambridge CB3 0HE, UK

8. PERFORMING ORGANIZATION REPORT NUMBER

RG 32402
October 2003

9. SPONSORING / MONITORING AGENCY NAME(S) AND ADDRESS(ES)

Research for US Navy, ONRRO, Boston, USA
Reports to: USARDSG-UK
223/231 Old Marylebone Road,
London NW1 5TH, UK

10. SPONSORING / MONITORING AGENCY REPORT NUMBER

11. SUPPLEMENTARY NOTES

12a. DISTRIBUTION / AVAILABILITY STATEMENT

Distribution unlimited

12b. DISTRIBUTION CODE

13. ABSTRACT *(Maximum 200 Words)*

In one series of experiments, see Sections 1-6, plasma/propellant interactions were studied. Four different propellants (see Section 3) were placed at chosen distances from the discharge. The discharges were made either in a high pressure vessel or at ambient pressures. In some cases, the propellant was at room temperature and in others at elevated temperature. Additionally, attempts were made to quench burning propellant. Optical and Environmental Scanning Electron Microscopy (ESEM), see Section 2.5, were used to study the propellant surfaces. Evidence was found for loss of material due to burning, droplets of the wire materials, fracture of the propellant surfaces, grain growth in the heated samples, bubble formation in the binder material and fibre-like structures and fern-like structures in the quenched samples. Of particular interest were the droplets which, from their appearance, had clearly impacted the propellant in the molten state. The remains of the droplets were often found in small craters suggesting that the molten wire material had caused reaction. The droplets ranged in diameter up to ~30 μm which is of the required size to cause ignition. Section 7 describes experiments on the deflagration to detonation transition (DDT). In addition to data on "conventional", so-called Type I DDT, we give evidence for a different mechanism (Type II DDT) which occurs with small particles packed to low density. Finally, an apparatus has been designed and built for studies of gas permeation through an explosive in granular form.

14. SUBJECT TERMS

Plasma, Propellants, Explosives, Deflagration to Detonation Transition, Microscopy

15. NUMBER OF PAGES 45

16. PRICE CODE

17. SECURITY CLASSIFICATION OF REPORT	18. SECURITY CLASSIFICATION OF THIS PAGE	19. SECURITY CLASSIFICATION OF ABSTRACT	20. LIMITATION OF ABSTRACT

Index

Abstract
In one series of experiments, see Sections 1-6, plasma/propellant interactions were studied. Four different propellants (see Section 3) were placed at chosen distances from the discharge. The discharges were made either in a high pressure vessel or at ambient pressures. In some cases, the propellant was at room temperature and in others at elevated temperature. Additionally, attempts were made to quench burning propellant. Optical and Environmental Scanning Electron Microscopy (ESEM), see Section 2.5, were used to study the propellant surfaces. Evidence was found for loss of material due to burning, droplets of the wire materials, fracture of the propellant surfaces, grain growth in the heated samples, bubble formation in the binder material and fibre-like structures and fern-like structures in the quenched samples. Of particular interest were the droplets which, from their appearance, had clearly impacted the propellant in the molten state. The remains of the droplets were often found in small craters suggesting that the molten wire material had caused reaction. The droplets ranged in diameter up to ~30 μm which is of the required size to cause ignition. Section 7 describes experiments on the deflagration to detonation transition (DDT). In addition to data on "conventional", so-called Type I DDT, we give evidence for a different mechanism (Type II DDT) which occurs with small particles packed to low density. Finally, an apparatus has been designed and built for studies of gas permeation through an explosive in granular form.

1. Introduction

The response of modern gun propellants is of increasing importance both for enhancing performance and ensuring safety in use and disposal. There have been several proposed schemes to improve the performance of existing and well-tested materials rather than developing more energetic, and potentially more expensive, alternatives. One of these proposals has been to introduce plasma into the burning front of a propellant grain, thus modifying the reaction kinetics and producing a burn that augments the pressures achieved and lengthens the pulse transmitted to the projectile. Traditional burning law equations were derived by Piobert (1839) and Vielle (1893) relating the rate of burn to the pressure and emphasising the role of the surface area of the burning region.

It is clear that the pressures and thus propellant gas-sound-speed achieved within a closed system (such as a gun breech) may be increased by simply heating the product gases by injection of hot plasma. This must be differentiated in any experimental investigation from alterations in the burning *rate* of the propellant.

Such effects have been tested in various laboratories at full-scale using modified gun breeches where plasma is injected in the form of jets from the vaporised liner of a glass tube. Although showing some increased performance over traditional systems, these experiments cannot differentiate between the various mechanisms of enhancement. Also the quantity of electrical energy required to gain significant performance increase is of the order of 10% of the chemical energy of the propellant.

Successful modelling has been performed on the high-voltage supplies for several such systems and on the plasma flows during injection. However, it is widely recognised that the greatest difficulty lies in successfully describing the plasma-propellant interaction.

In research on this contract, a simple, well-controlled test apparatus is being developed and used to study the burning properties of a propellant grain with and without injected plasma. The equipment allows the amount of electrical energy introduced to be varied and precise control of the geometry of the plasma relative to the burning front to be obtained. This system has the flexibility to allow control of the plasma injection in a simple geometry that should be accessible to analytical modelling. The aim is to measure the enhancement at a particular pressure and

propellant burn-rate. Experiments have been made of propellant at ambient temperature and heated propellant. Additionally, attempts have been made to quench the burning propellant and to study the reacted surface.

Extensive use has been made of microscopy both optical and ESEM (Environmental Scanning Electron Microscopy). This has shown that when, for example, tungsten wires are used that there are contributions to the ignition from both the plasma and also droplets from the wire material.

The transition from burning (deflagration) to detonation (DDT) has also been studied. Observations on "normal" DDT, so-called Type I are presented as well as a new form of DDT, so-called Type II. Type II is important for low density, small particle size, powders.

Experiments were also started on the propagation of gaseous products through a bed of particles. These data are important if DDT is to be successfully modelled.

2. Equipment

2.1 Pressure Vessel

Figure 1 shows the pressure vessel used for the research. The system consists of a closed reaction vessel capable of withstanding high static pressures, 10,000 atm. It is fitted with a pressure gauge with a time resolution 5 μs.

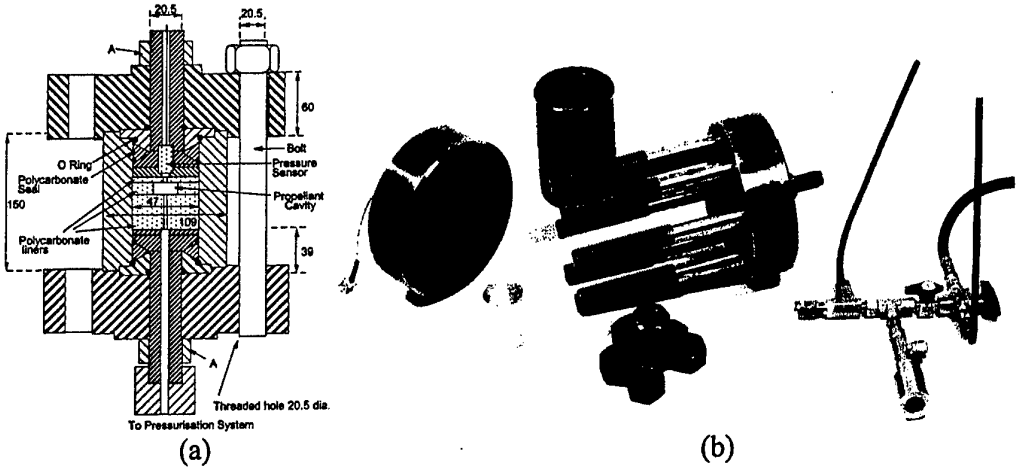

Figure 1. (a) Cross-section of pressure vessel; (b) Photograph of the disassembled cell.

The cell has been designed to allow propellant grains to be burned in a chosen volume configuration. Typical traces are given in Figure 2.

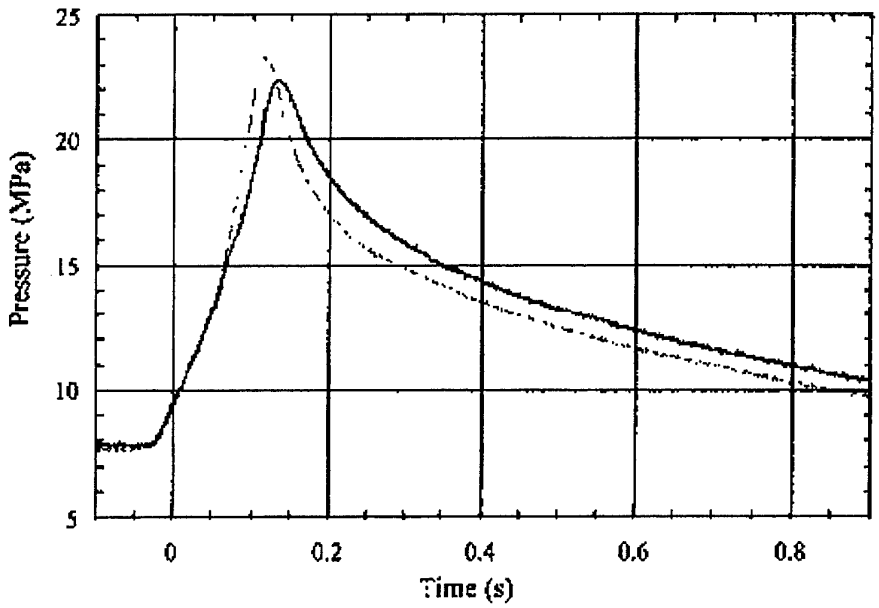

Figure 2. Pressurisation graph of the cell. Pyrophyllite liners giving 15 cm^3 internal volume, 1g NQ/T propellant. The traces are for two separate experiments.

One of the main questions is the nature of the interaction between the plasma and the burning propellant. Does the plasma get chemically involved or does the expanding plasma break up the surface causing extra surface area to be revealed? The bursting diaphragm system, see Figure 3, has been tested using copper diaphragms of differing thickness between 0.025 – 4.00 mm. In the clamping system used, this allows the diaphragm to burst at chosen pressures between 5 – 250 atm. This allows the system to vent when only small amounts of material are burned either at atmospheric pressure or with substantial pre-pressurisation. The ejected fragments are caught by a catcher system, which can be filled with liquids or solids to help quench the reaction.

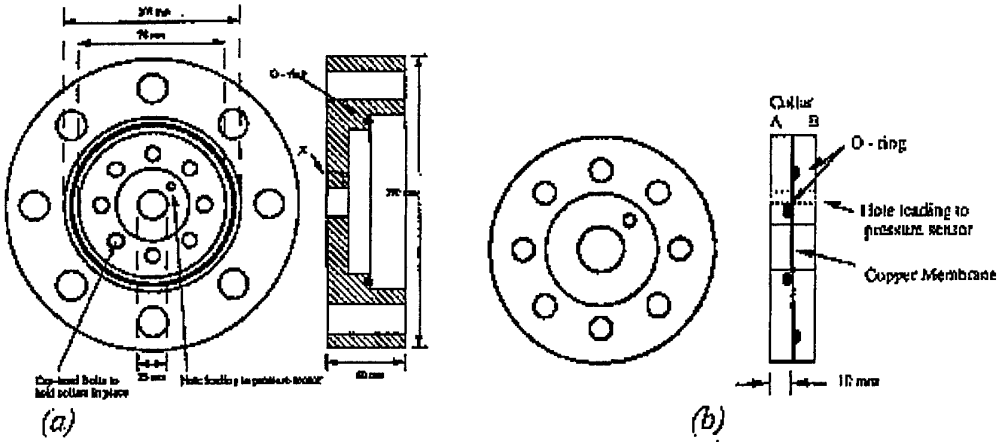

Figure 3. The bursting disc flange. (a) General cross section, (b) collar used to hold bursting disc.

Typical current/time, voltage/time traces are shown in Figure 4.

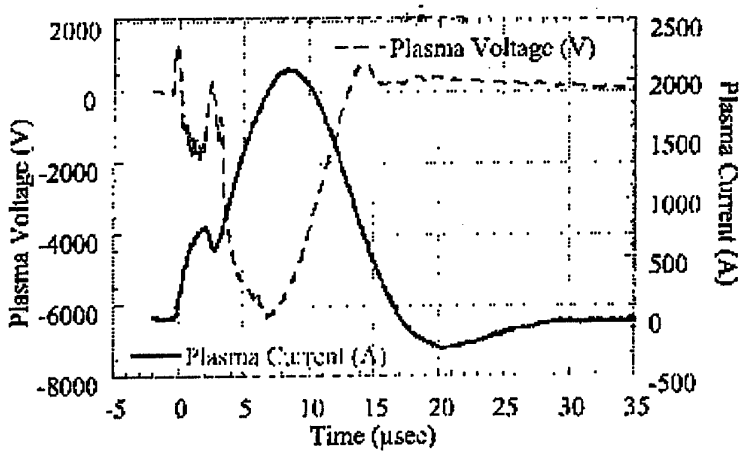

Figure 4. Discharge profile for tungsten wire, 5 kV charge, 70 J in 20 μs.

2.2 Discharge Equipment

This consists of a capacitor bank with various options for the capacitance, a charging control panel, a discharge chamber and two oscilloscopes.

A schematic of the experiment is shown in Figure 5 and pictures are given in Appendix A. The capacitor bank is connected to a Charging Control Panel which is used to select the energy stored in the capacitor bank. The voltage can be varied between 1-10kV and the capacitance in steps from the minimum of 892pF to a maximum of 87.622nF. The total energy delivered in the system is derived from the equation $(CV^2)/2$.

The capacitor bank is also connected to the discharge chamber where the behaviour of the energetic materials is studied. The discharge chamber is made of polycarbonate and is strong enough to survive any detonation or blast wave generated by the secondary explosive or propellant involved.

The capacitor bank is fitted with a voltage monitor and a Rigowsky coil. The out-puts go to two oscilloscopes. The first oscilloscope is set to measure the voltage and current histories on a long timescale of 20μs. The second oscilloscope measures these voltages at a shorter timescale of up to 10μs.

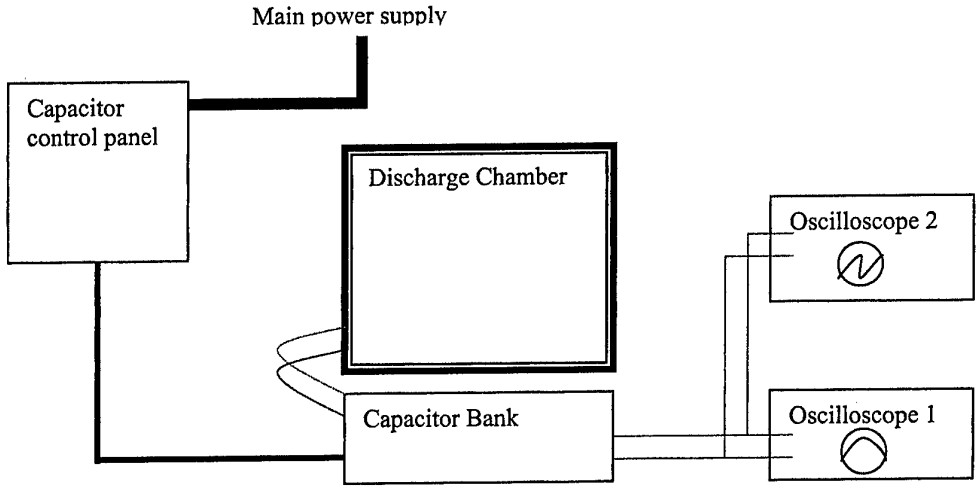

Figure 5. The set-up of the discharge experiment.

Figure 6 shows the ignition circuit used. Figure 7 shows the potential divider used to step down the voltage by a factor of ten before recording. A 0.10 ± 0.05 mm diameter, 2.5 ± 0.5 cm length tungsten wire was placed across two carbon electrodes connected via a trigger system to a 5000 V supply. Samples of propellant were placed in a 25.00 ± 0.02 mm circular sample holder, filling a 2.8 ± 0.1 mm hole and positioned vertically at distances of 0, 1 and 5 mm from the wire. The holder set-up was such that the centre of the holder lay level with the height of the wire.

The circuit was then triggered so that the 5000 V supply was put across the tungsten wire creating the plasma that interacted with the surface of the propellant.

The resulting voltage produced in the experiment was then sent through the potential divider, which stepped down the voltage by a factor of ten, to a CRO. The trigger system used allowed the current passing through the circuit to be displayed at 0.1 VA^{-1} on the voltage trace.

The resulting voltage trace was then recorded in a spreadsheet and corresponding actual voltage (voltage trace × 10) and current voltage (voltage trace × 100) calculated.

Using these results, a power-time curve was created where $P = IV$. An example of the resulting plots is shown in Figure 8. Using the package, Kaleidograph, the area under the curve was integrated to find the total energy of the explosion.

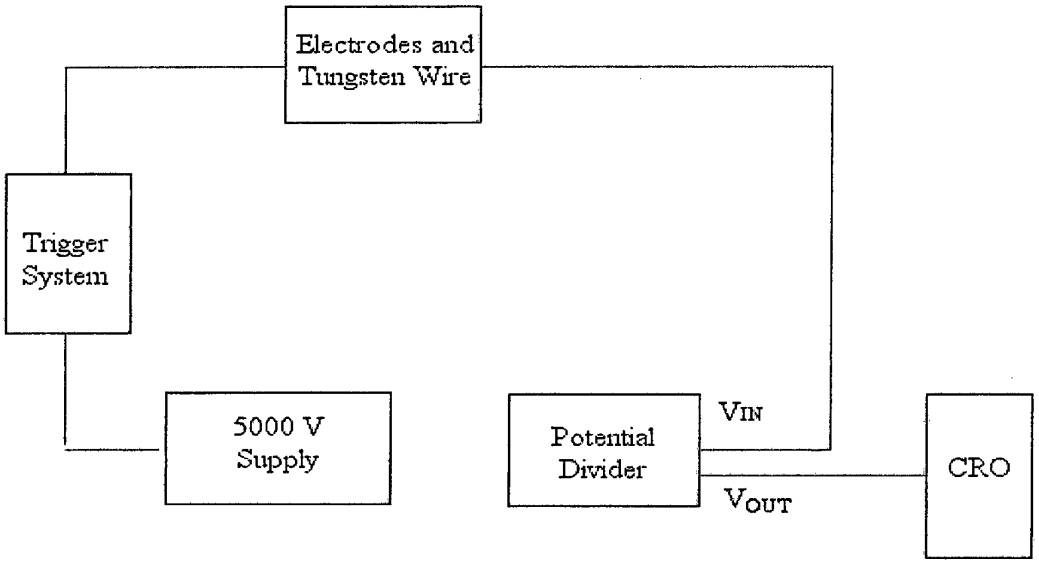

Figure 6. The ignition circuit used.

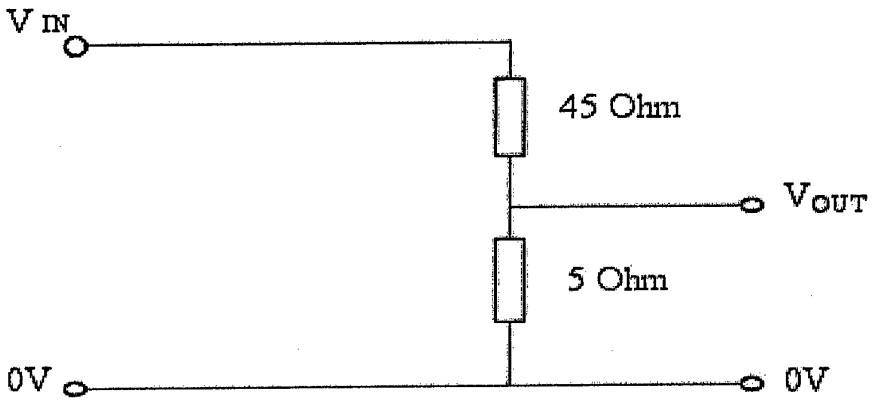

Figure 7. The potential divider circuit.

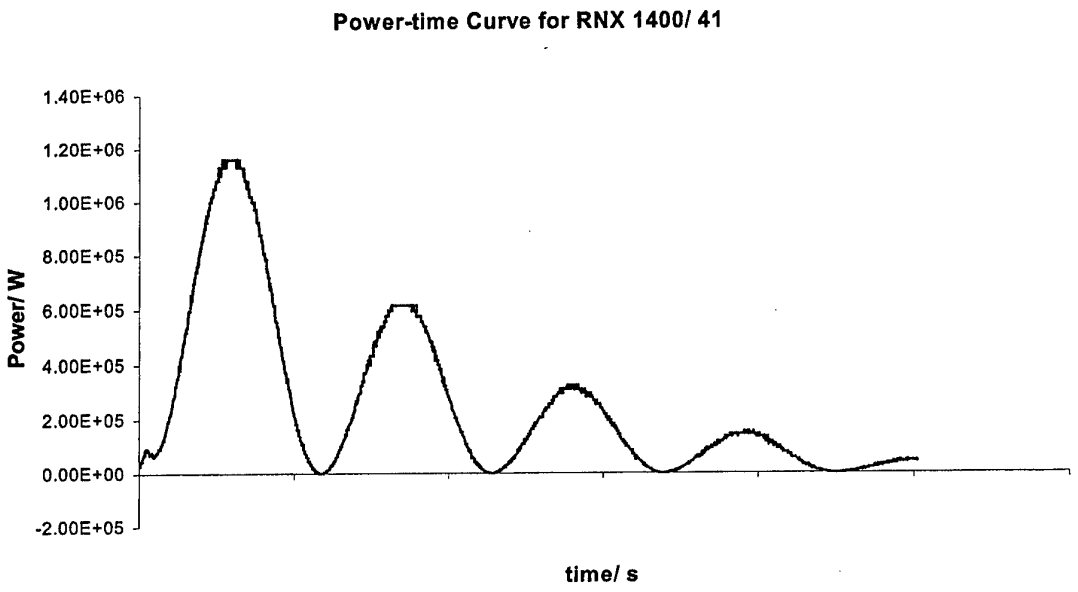

Figure 8. Sample power curve obtained.

2.3 Heated Samples

Samples of the propellants were placed into similar copper sample holders. These were positioned onto a hot plate on top of a 5 × 5 cm square copper plate and heated until they reached their burning temperature. The temperature at which this occurred was measured using thermocouples, one beneath the sample holder and one beneath the copper plate in order to check whether there was a significant temperature gradient across the copper sample holders.

Once the burning temperature had been established, new samples were placed onto the hotplate in the set-up shown in Figure 9 and heated to 160, 180 and 200 °C, all below their burning temperatures. When the desired temperature had been reached, a piece of the same tungsten

wire was placed between the contacts in a sharp loop and placed in contact with the propellant surface and reaction started.

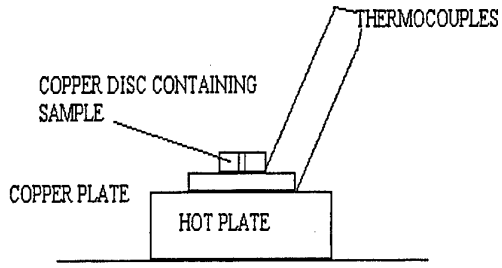

Figure 9. The hot plate set-up.

2.4 Liquid Nitrogen Quenching of Samples

In these experiments, samples were heated using the same hot plate set-up until they were just on the point of combustion. Using a thin membrane, which burst on triggering the tungsten wire, liquid nitrogen was deposited onto the heated sample thus quenching the reacting material.

2.5 Environmental Scanning Electron Microscope (ESEM)

A considerable disadvantage with a conventional SEM is the necessity for the specimen surface under examination to be conducting. This problem can be overcome with the use of an ESEM (Farley & Shah 1991; Danilatos 1993). In the ESEM, this limitation of a conventional high-vacuum SEM with regard to insulating samples is removed by the utilization of residual gas in the specimen chamber. Gas pressures of between 1 and 20 torr are maintained in the specimen chamber, which is separated from the high-vacuum electron column by several pressure-limiting apertures.

A traditional high-energy electron beam (2-30 keV) is used to scan the sample generating secondary and back-scattered electrons from the specimen surface. A sufficient positive potential is maintained on a detector above the sample to accelerate these emitted electrons upwards. If the electrons gain sufficient energy, interactions with residual gas molecules cause extra electrons with a few eV of energy to be released and positive gas ions to be created. This interaction may happen many times on the way to the detector. The positively ionised gas molecules bombard regions of negative charge build-up on the specimen surface in a self-regulating manner so that the surface remains neutral. Additionally, the avalanche effect caused by the electron-gas interaction causes a signal magnification at the positively biased detector (figure 10). For a more detailed explanation of the gaseous-amplification and contrast-forming mechanisms, see Thiel *et al.* (1997) and Stokes *et al.* (1998). Examples of ESEM pictures of deforming PBXs can be found in Rae *et al.* (2002).

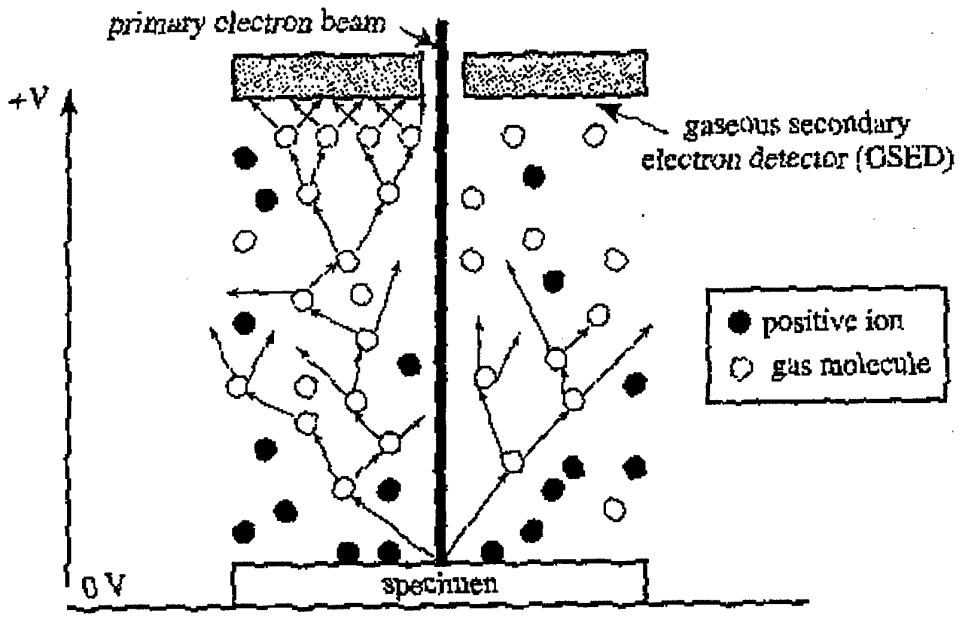

Figure 10. Illustration of the gaseous-amplification effect in the ESEM (after Thiel *et al.* 1997).

3. Materials

The four propellants are described in Table 1. Samples were cut from larger blocks.

Propellant	Composition
Rowanex (RNX) 1400	66% RDX, 22% Al, 7% plasticiser, 5% binder
Rowanex (RNX) 3000	95% HMX, 5% HTPB
RF69	35% RDX, 60% TATB, 5% binder
RF38	Similar to RG69; differences not known

4. Microscopy of Surfaces

4.1 Wire in contact with the surface; explosive at 291K

The discharge caused typically 400 μm of material to be removed. There was evidence of solidified molten droplets along the path of the discharge. Examples are given in Figure 11 (a droplet is arrowed) and Figure 12 taken at a higher magnification. Droplet diameters range from 1 to 8 μm.

Figure 13 is interesting in that it shows a droplet which has impacted and spread on the surface of the PMMA holder. Its average diameter is ~30 μm.

4.2 Wire 1mm above the surface; explosive at 291K

The amount of material removed by reaction was very small and typically just a few μm. Figure 14 shows a great many droplets along the path of the discharge which was horizontal across the picture.

Figure 15 is at a higher magnification. The largest droplet has a mean diameter of ~4.4 μm and the medium sized droplet 1.66 μm.

4.3 Wire 5mm above the surface; explosive at 291K

Figure 16 is an example where the surface of a large crystal fills most of the field of view. A molten drop appears at the right-hand side of the picture. Note the presence of holes (some are arrowed) of similar size to that of the droplet.

4.4 Wire in contact; explosive at high temperature

At higher temperatures, the surface shows evidence of texture changes due to melting. The example, at T = 453K (Figure 17) has several cases of droplets in holes. Two examples are arrowed: the droplet is at the centre of the hole suggesting the droplet caused some local decomposition.

Figure 18 shows a sample held at 473K before discharge. There are various cases of particles in holes; three are arrowed. In general, the holes are much larger compared with the droplets than in examples at lower temperatures.

4.5 Debris from wire?

Figures 19 and 20 show examples of flakey-type deposits which may have come from the tungsten wire. Currently we are trying to identify the material using X-rays.

Much research in the area of plasma/propellant interactions assumes it is the high temperatures from the plasma which causes and/or enhances the explosive reaction. However, in the experimental situation described in this report there is clear evidence for the wire producing high temperature droplets. The wire may also produce hot debris though X-ray analysis is needed to identify the fragments, seen, for example, in Figures 19 and 20.

The melting point of tungsten is very high (3680 ± 20K). The spherical shape of the droplets suggests that the ejected particles must be near their melting point. At least near enough that surface tension can make the droplets spherical. These surface forces are, of course, more significant for smaller droplets.

However, the temperatures reached are likely to exceed the "hot spot" temperatures required for ignition of the explosive. Also their sizes (up to ~ 30 μm) are of the required size.

Evidence that they cause reaction is provided by the holes found on the surface. Several holes have the remains of a droplet at their centre. In cases where the sample was at a high temperature these holes were relatively large (see Figure 18) indicative of more reaction.

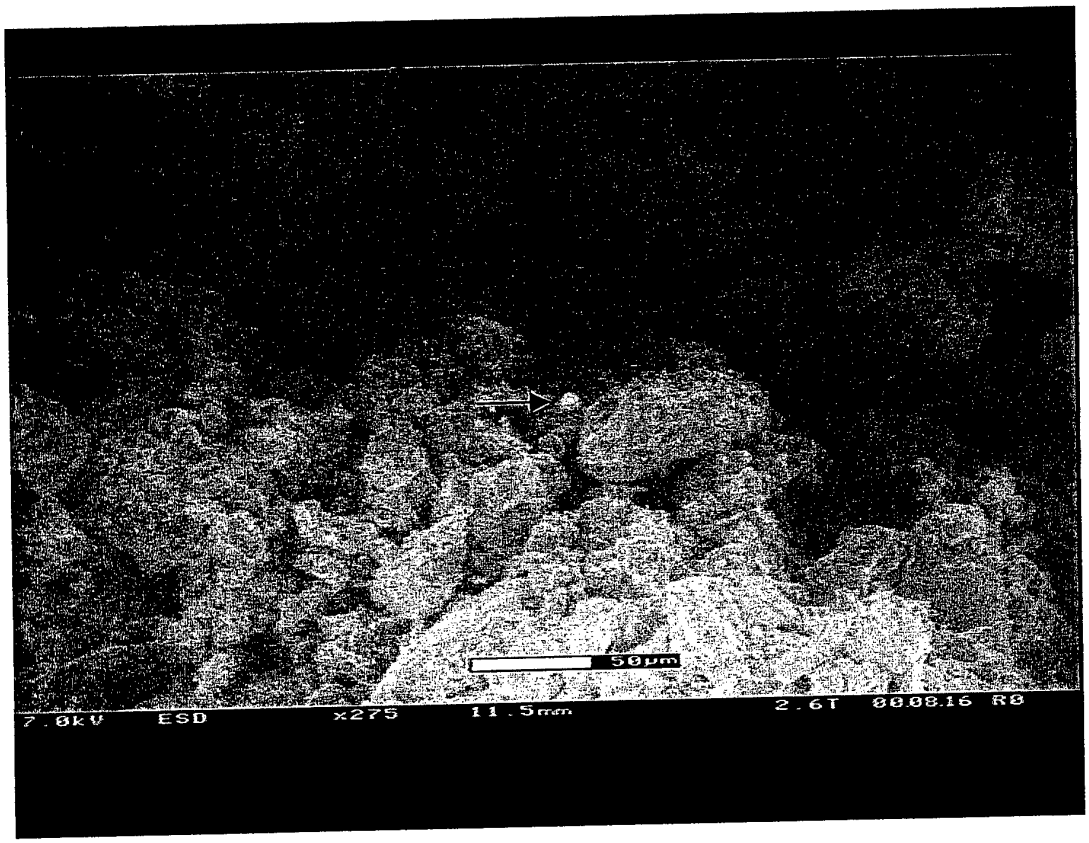

Figure 11. A tungsten droplet on the surface of the energetic material.

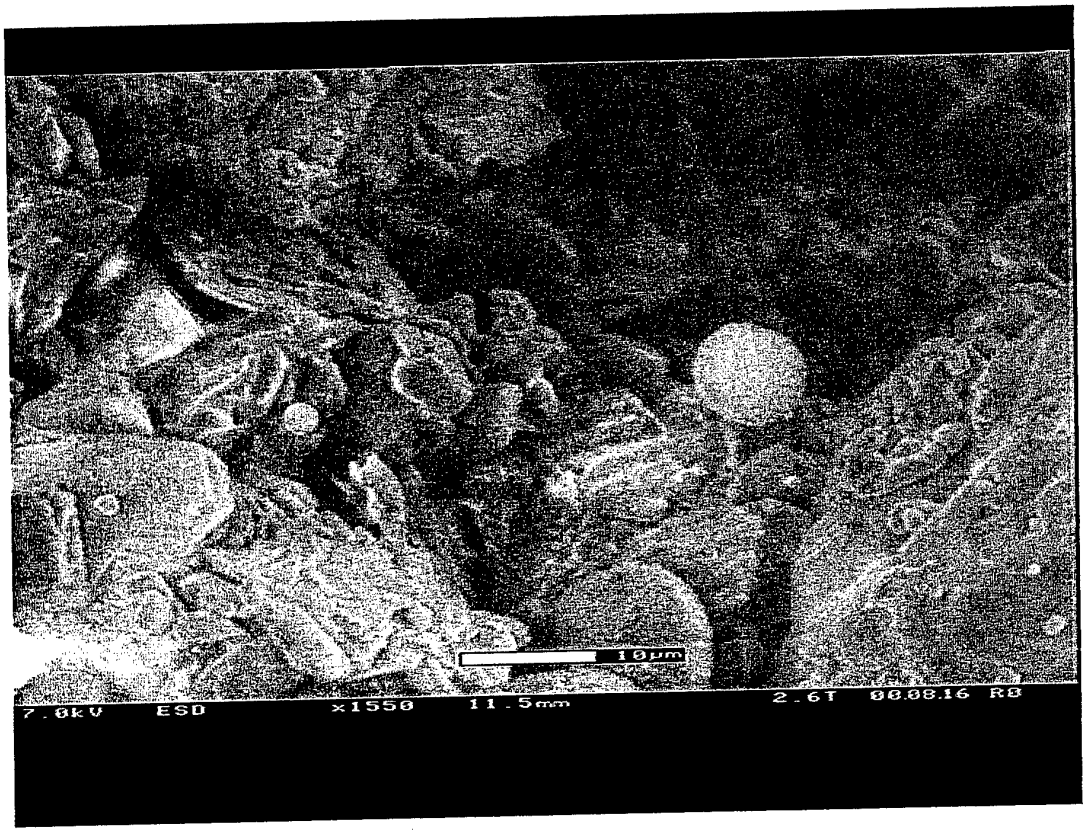

Figure 12. Solidified droplets of tungsten on the material. There are a wide range of droplet sizes.

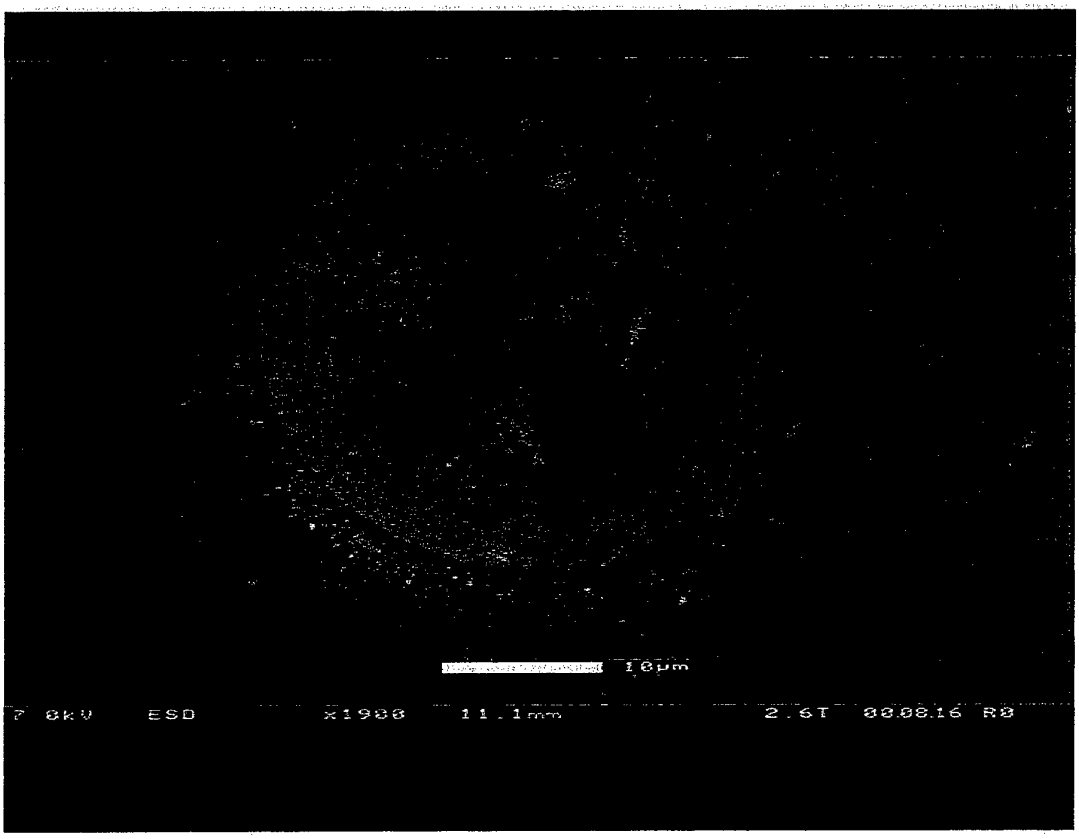

Figure 13. Soldified tungsten droplet on the PMMA holder.

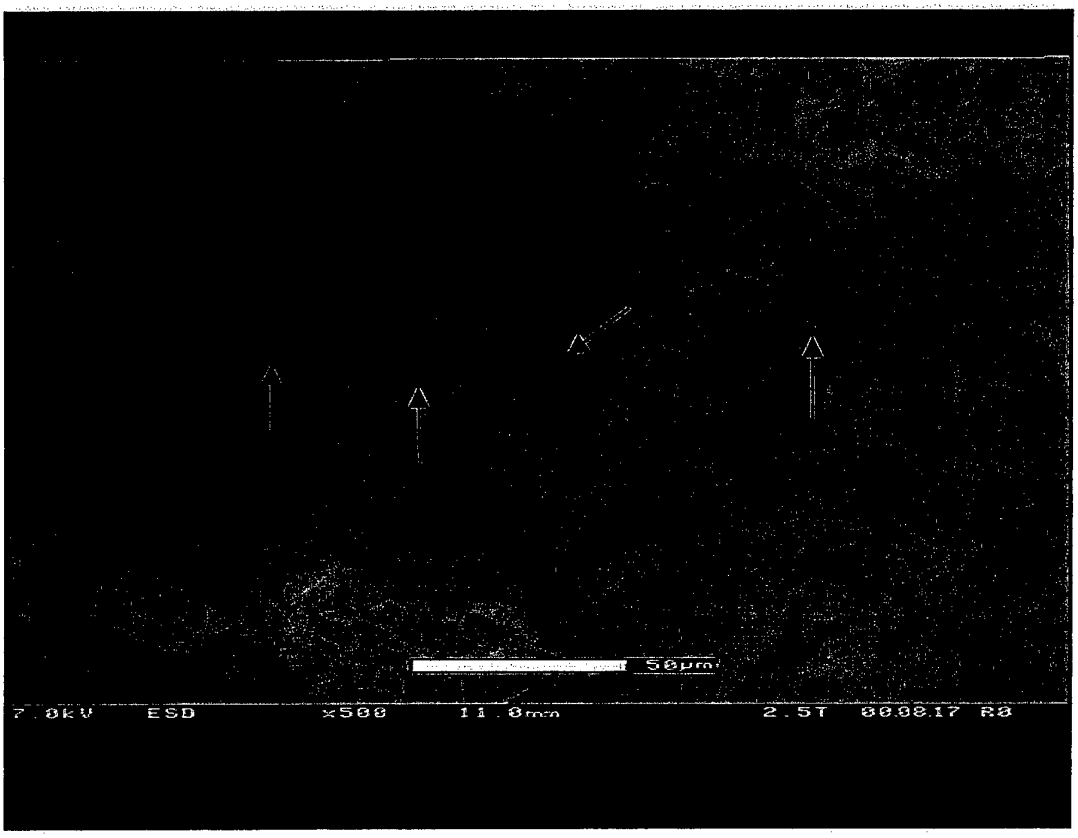

Figure 14. Tungsten droplets scattered on the surface of the energetic material along the projected path of the discharge.

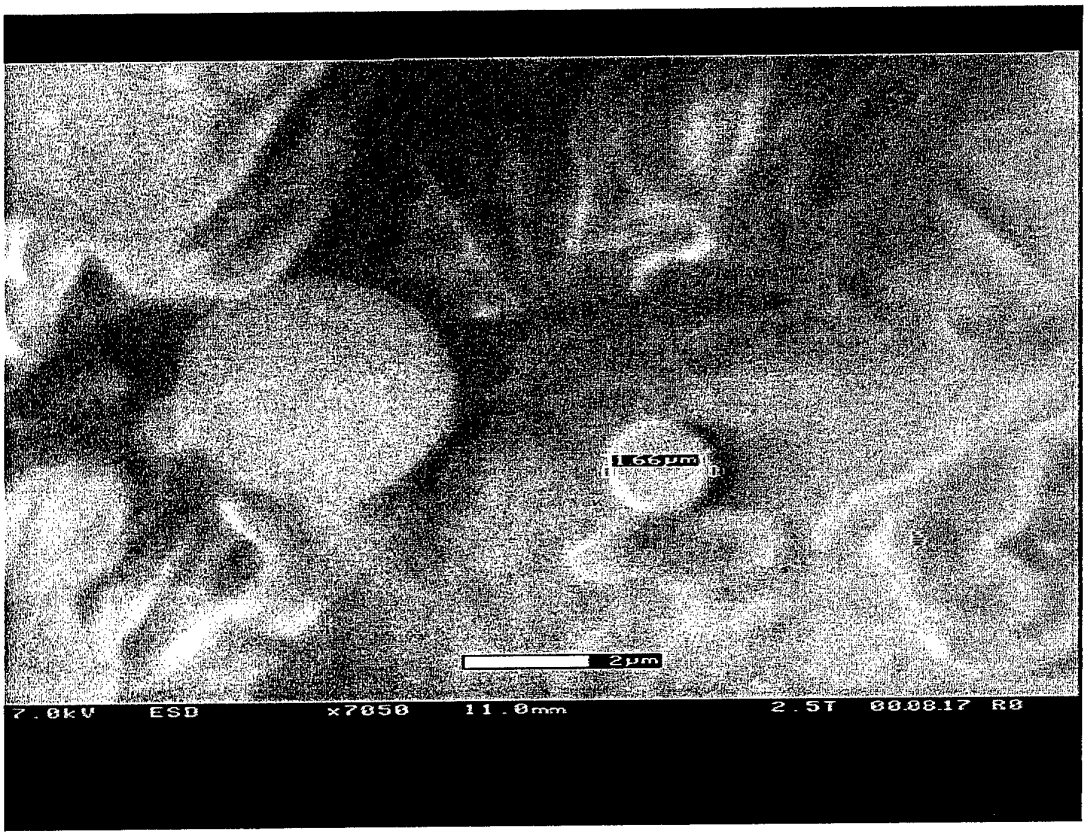

Figure 15. Picture at higher magnification.

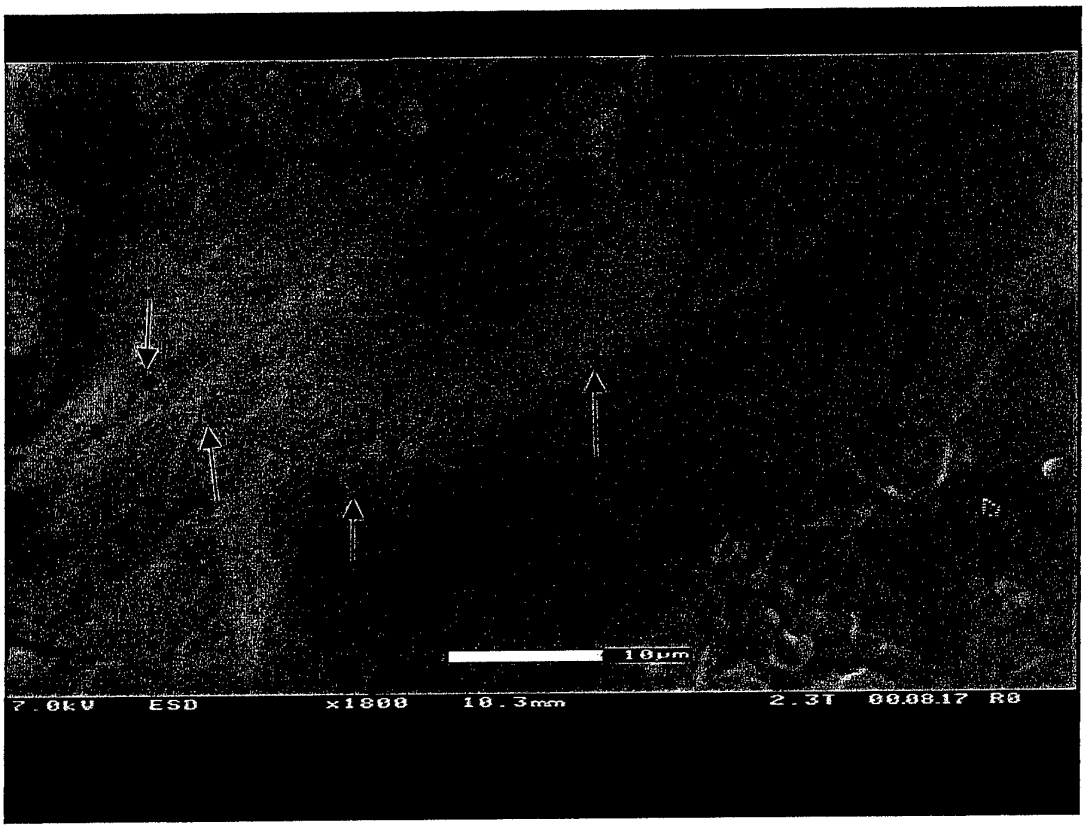

Figure 16. A crystal can be seen with small "holes" scattering over its surface. On the far right a tungsten droplet can also be seen.

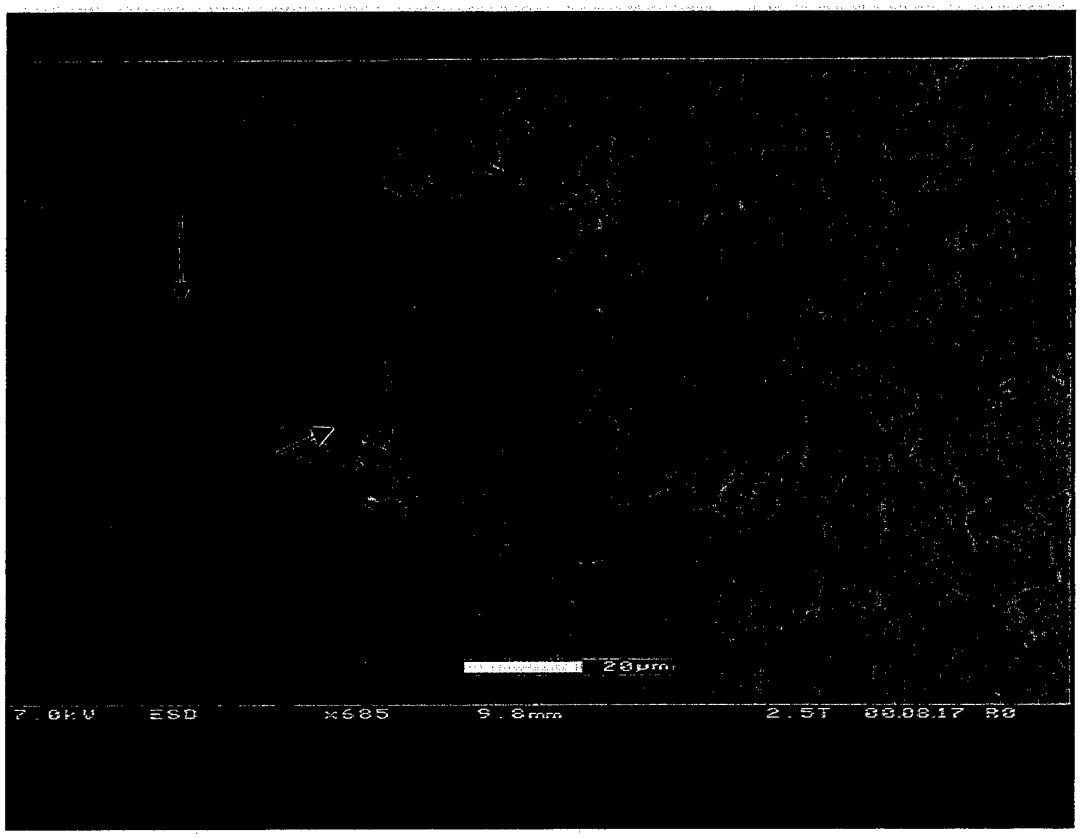

Figure 17. Sample is at 453K. Several cases of particles in holes; two are arrowed.

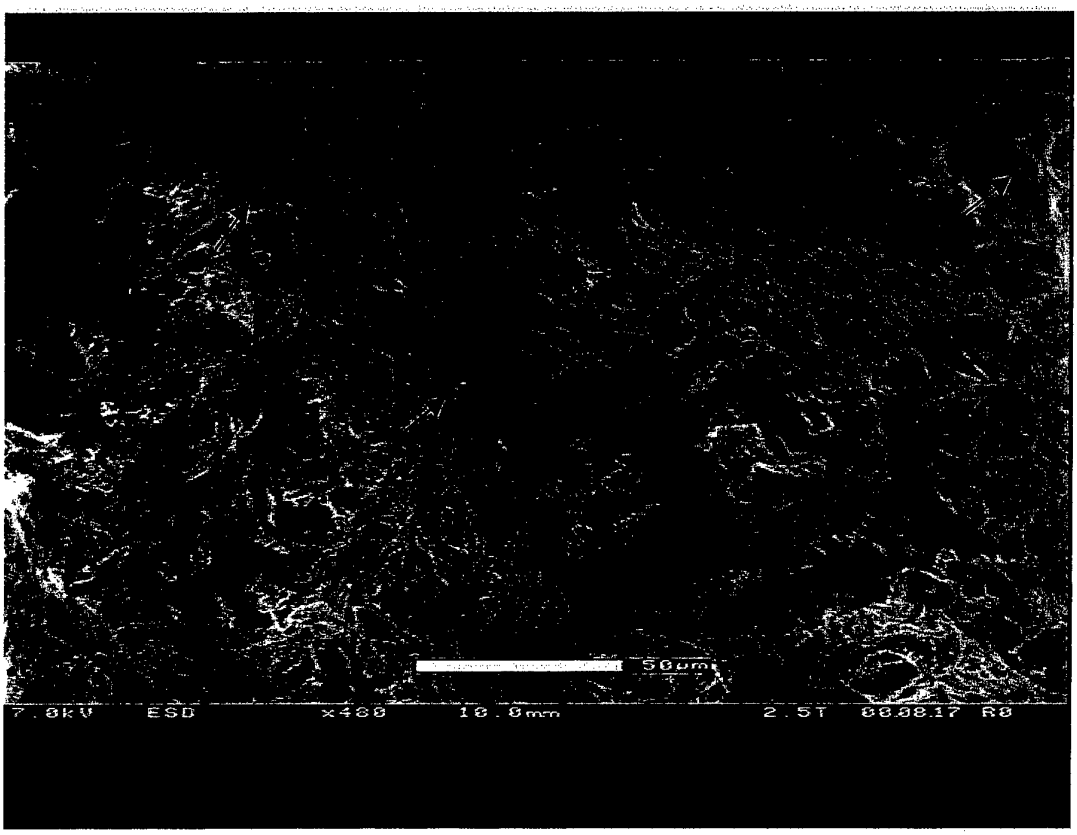

Figure 18. The sample was at 473K. Again there are many cases of holes with droplets near the centre. At this temperature the holes are much larger than the droplets indicating more reaction.

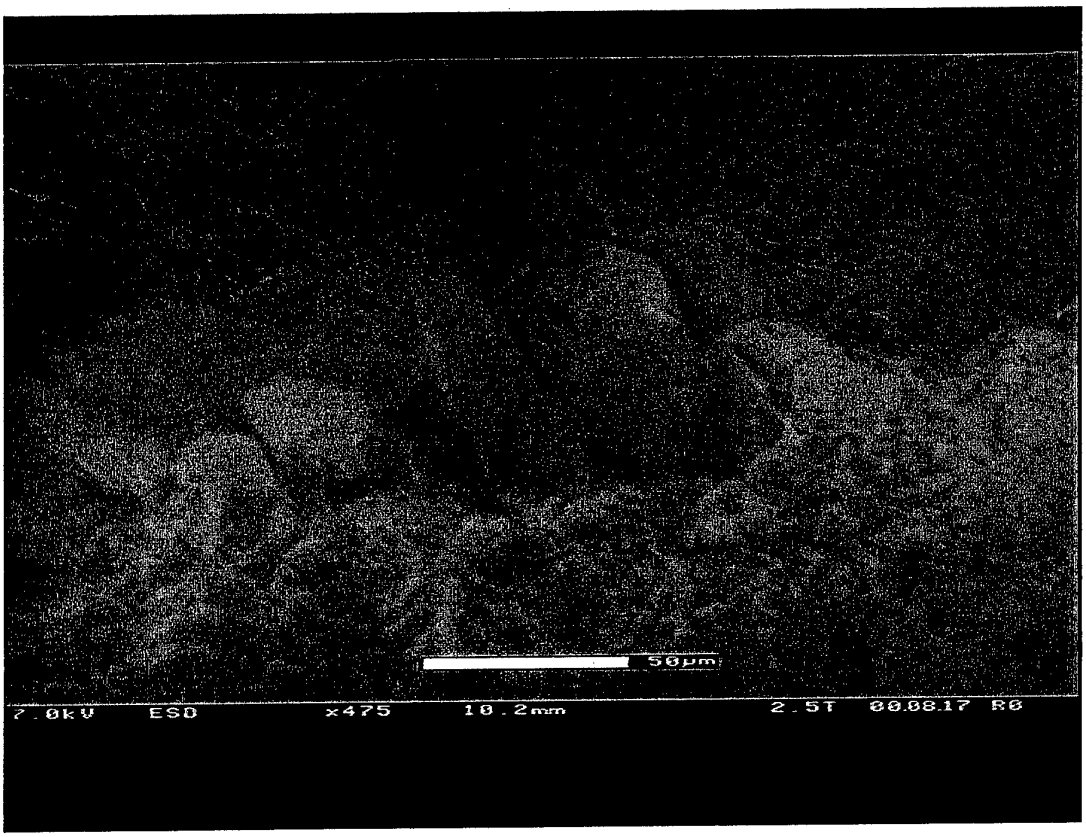

Figure 19. Possible debris from wire. Sample at 473K. Wire in contact.

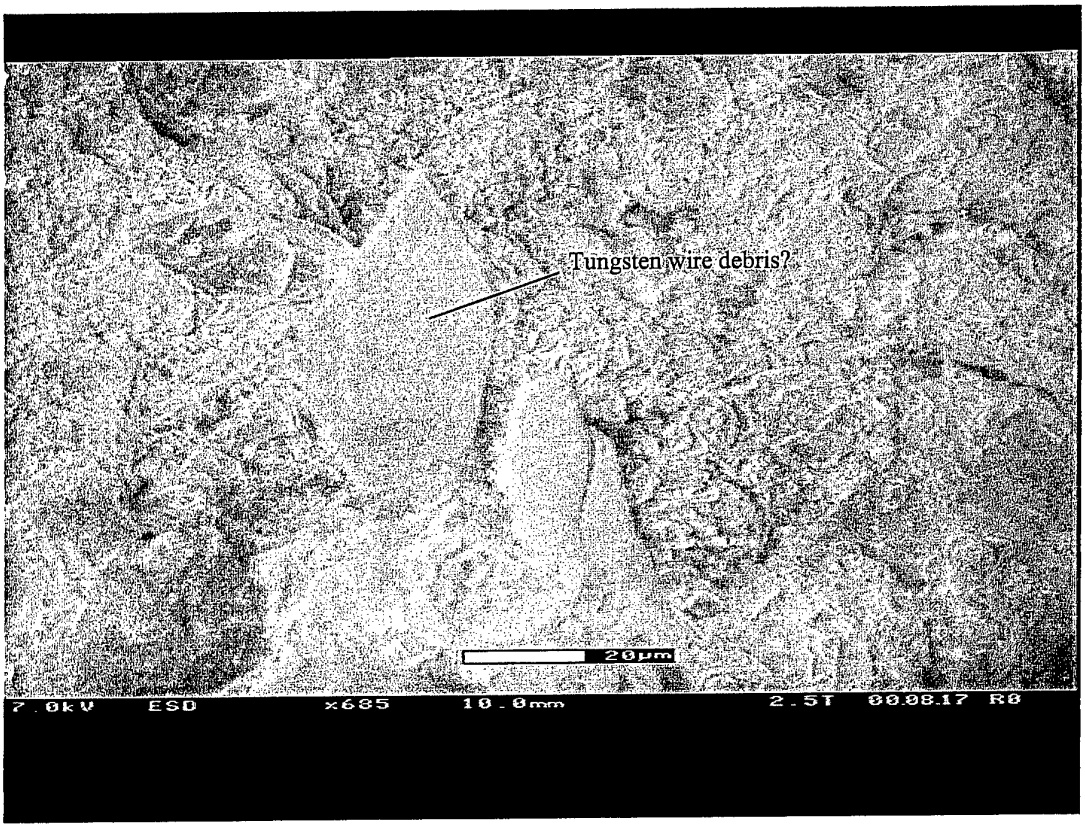

Figure 20. Possible debris from tungsten wire. Sample at 453K. Wire in contact.

5. Room Temperature Samples

Figures 21-24 show the digital photographs taken of damage to the surfaces of room temperature propellant samples. Features observed include large crystalline structures, wire on the surface, surface burning and evidence of the propellant being blown away from the sample holder following reaction.

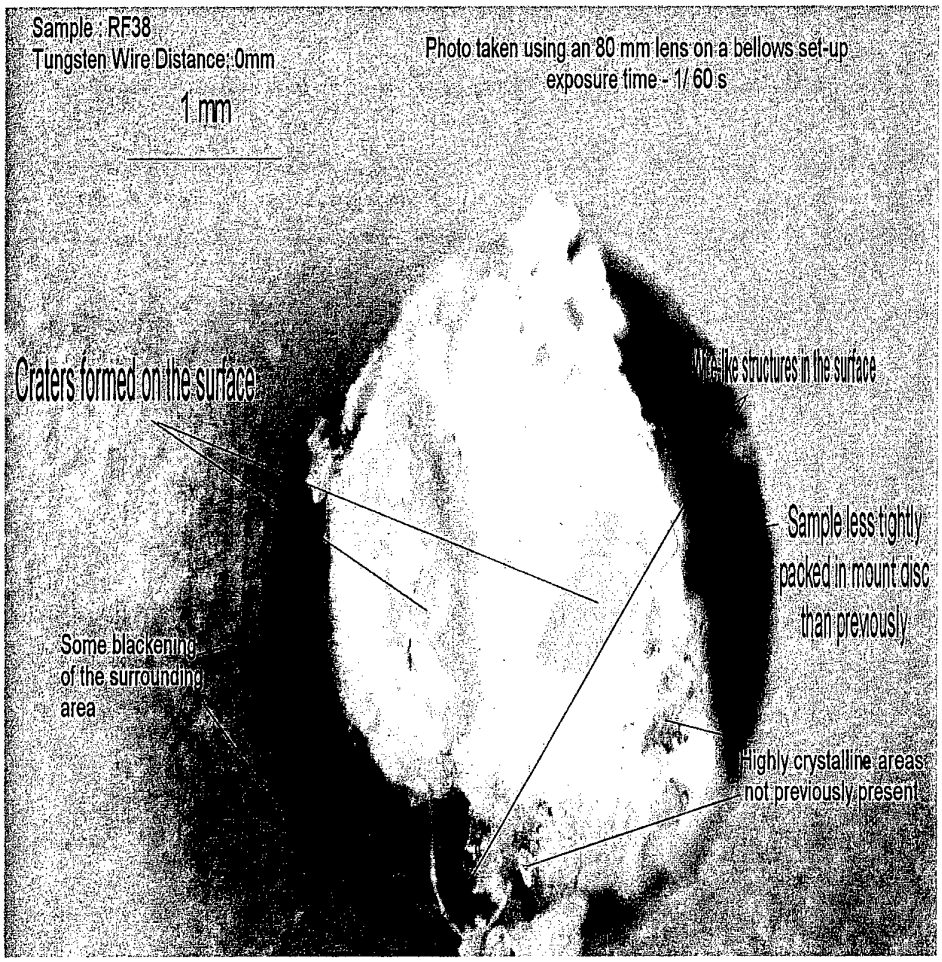

Figure 21. Optical microscopy image of RF38.

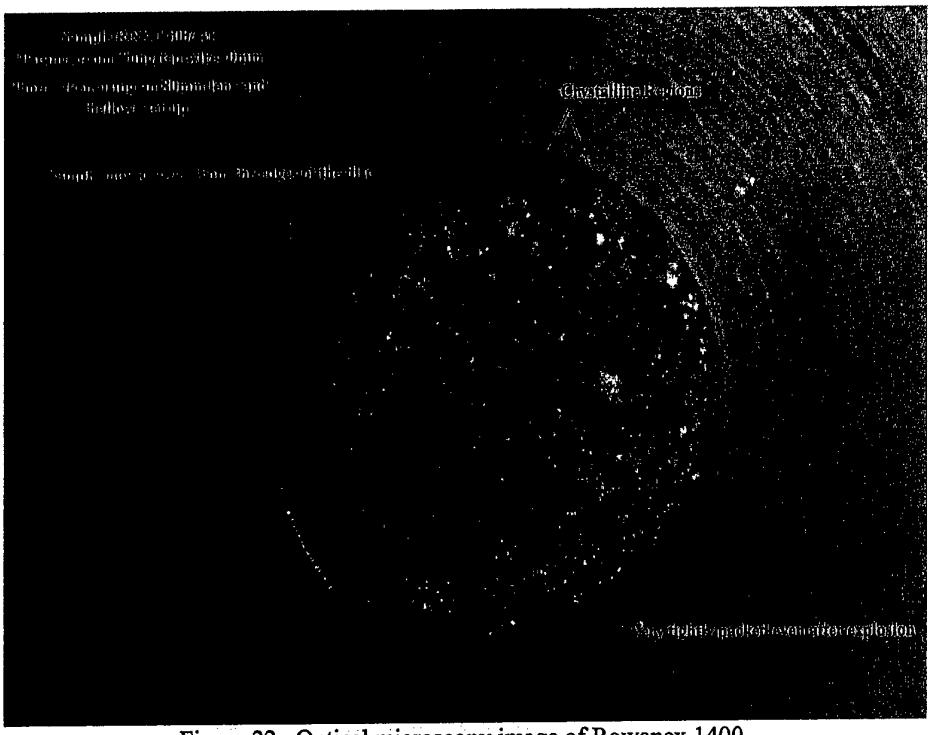

Figure 22. Optical microscopy image of Rowanex 1400.

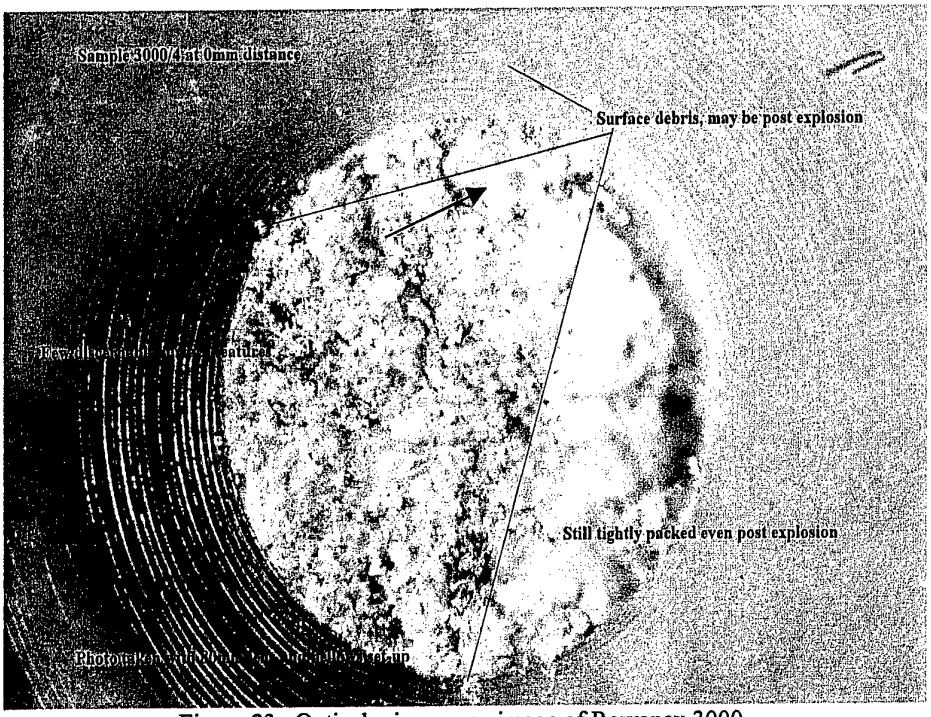

Figure 23. Optical microscopy image of Rowanex 3000.

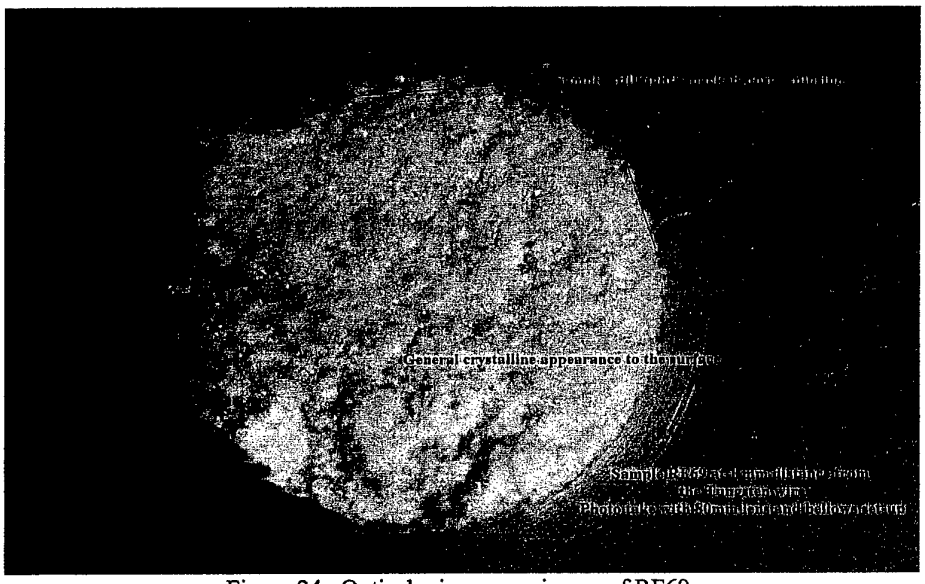

Figure 24. Optical microscopy image of RF69.

Figures 25-27 show the images taken with the ESEM, scale bars indicate the size of the structures present. The major features present are circular droplets of tungsten, between two and five microns in size, (Figure 25). The surface near where the hot tungsten deposited usually shows evidence of melting and pitting.

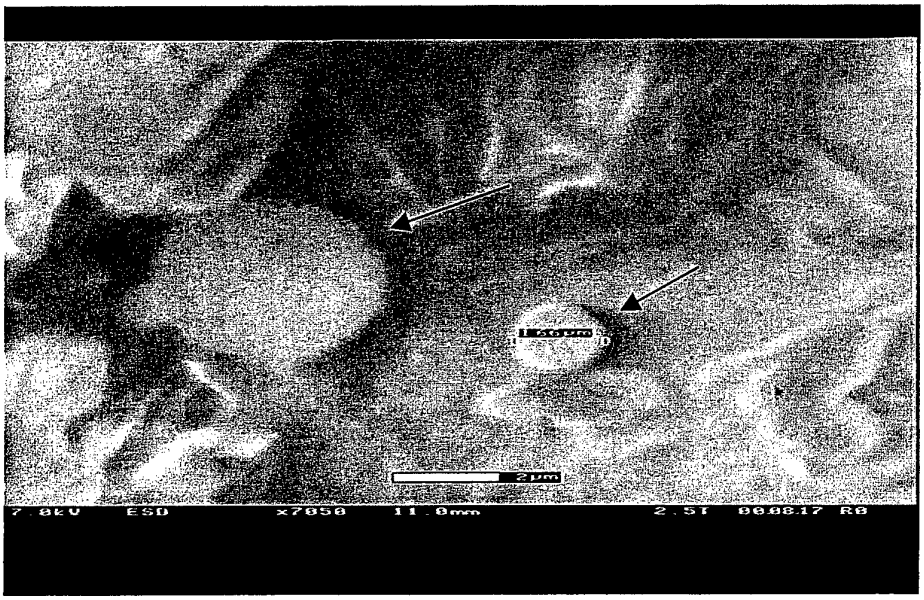

Figure 25. ESEM image of two tungsten droplets arrowed, 7050x magnification marker shows extent of droplet. Material is RF69.

Figures 26 and 27 give evidence of plasma discharge, melting and decomposition.

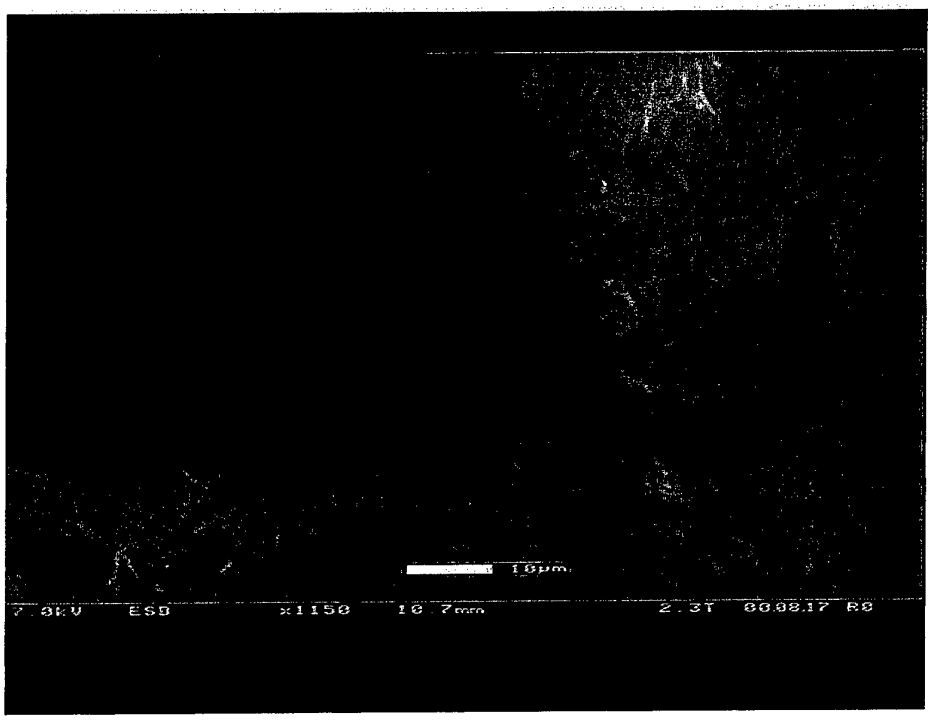

Figure 26. Damaged crystals throughout the melted background (sample RF69).

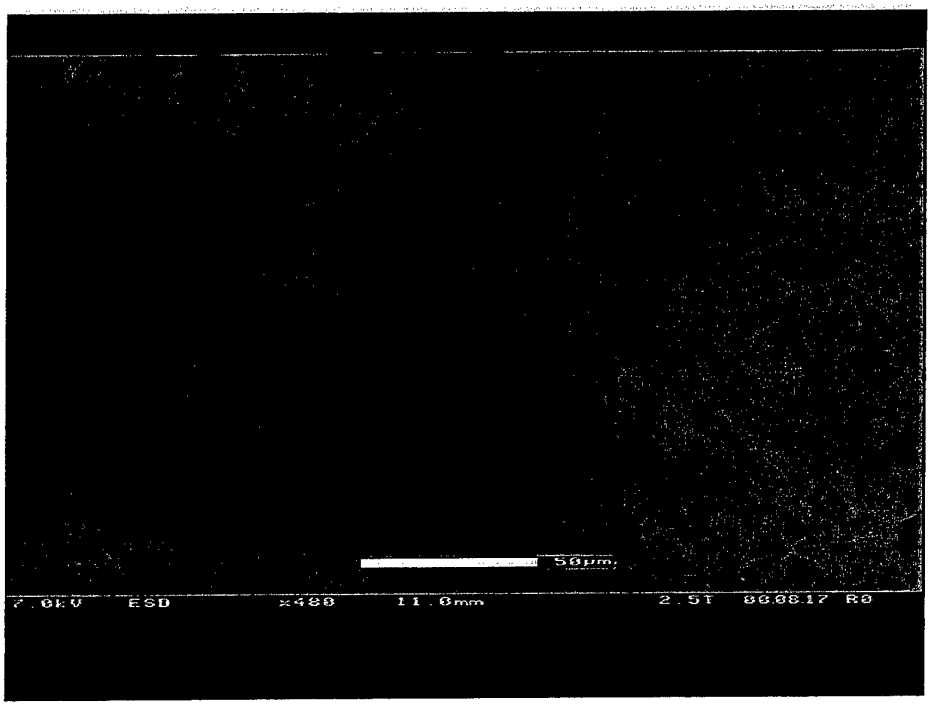

Figure 27. General background area of RF69 propellant.

5.1 Results from Heated Samples

The results from the heated samples were also analysed using the ESEM. The temperatures recorded for burning were 259 °C and 267 °C for RF69 and Rowanex 3000 respectively.

ESEM images (Figures 28-30) suggest that a larger degree of damage was done to these pre-heated samples. Once again some large crystals were seen in the images. These larger crystals appear to be more prevalent than in the virgin material suggesting grain growth during the heating.

Tungsten droplets were observed on these samples. Near these rounded structures there was evidence of melting and decomposition thus supporting earlier observations.

Examining samples which were heated to the point of combustion several new features were observed including layered structures, exceptionally smooth crystals, fern-like growth patterns and bubbles. The vast majority of these bubble-like structures appeared to be points where the sampled had bubbled up and then during cooling the bubble, presumably of binder material, had shattered. They were noted to be extremely thin, as demonstrated by their transparency and to be almost perfectly spherical.

Figure 28. Large crystalline structures found burnt and fired samples. Sample RF69, heated to 181 °C before plasma discharge.

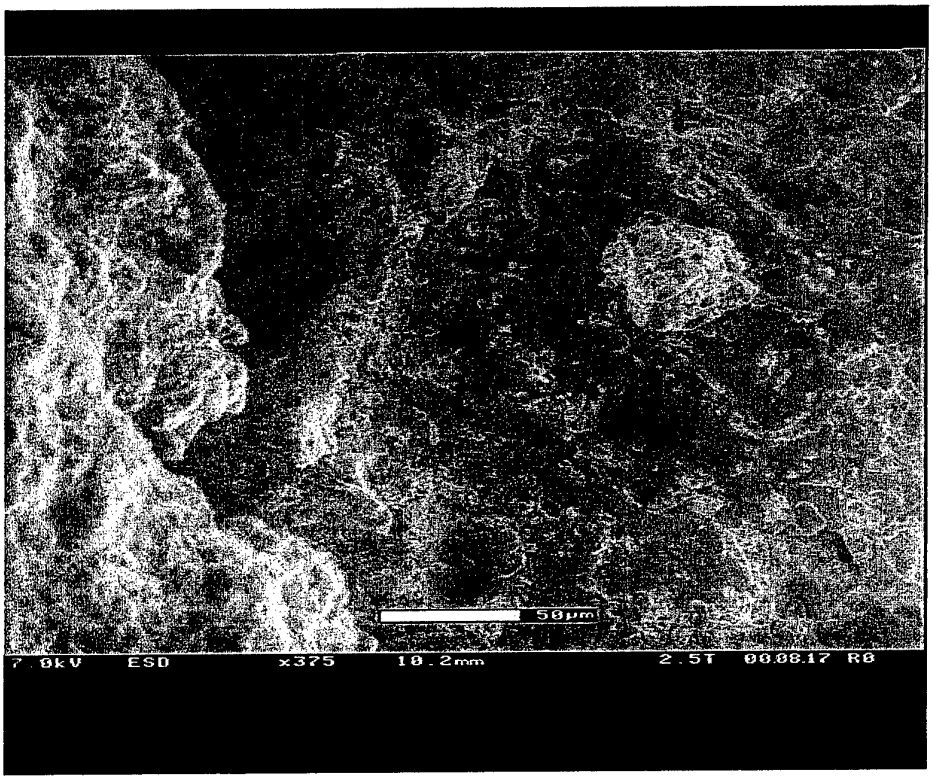

Figure 29. Surface marked with deep pits (RF69).

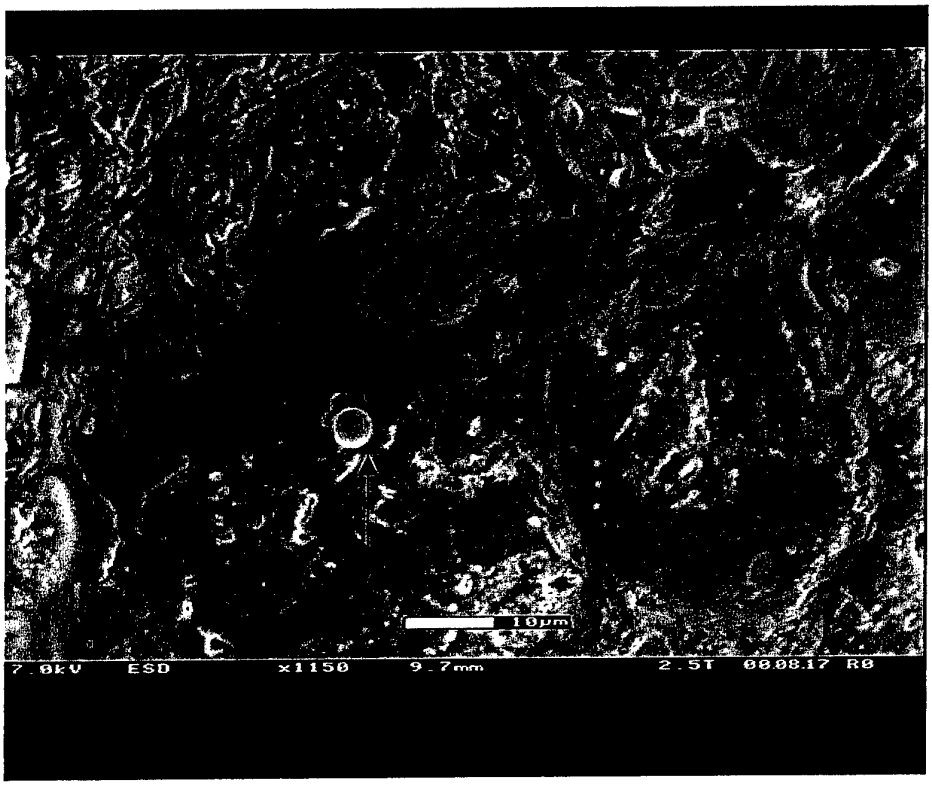

Figure 30. Tungsten droplet arrowed and its position in the sample of RF69, demonstrating the area of melt around it.

Figures 31-37 show the damage inflicted on the samples which were heated to their burning temperatures. Figures 31 and 32 show bubbles which have fractured and Figure 33 a complete bubble. Figures 34 and 35 show crystals found in the structure which are much larger than previously seen in the background matrix suggesting that a recrystallisation process probably takes place upon heating. Figure 36 shows a fern-like growth structure, again probably an indication of recrystallisation of material on heating. Finally, Figure 37 shows an example of the loops of material (not thought to be from the tungsten wire) found in some of the ESEM pictures of this particular sample.

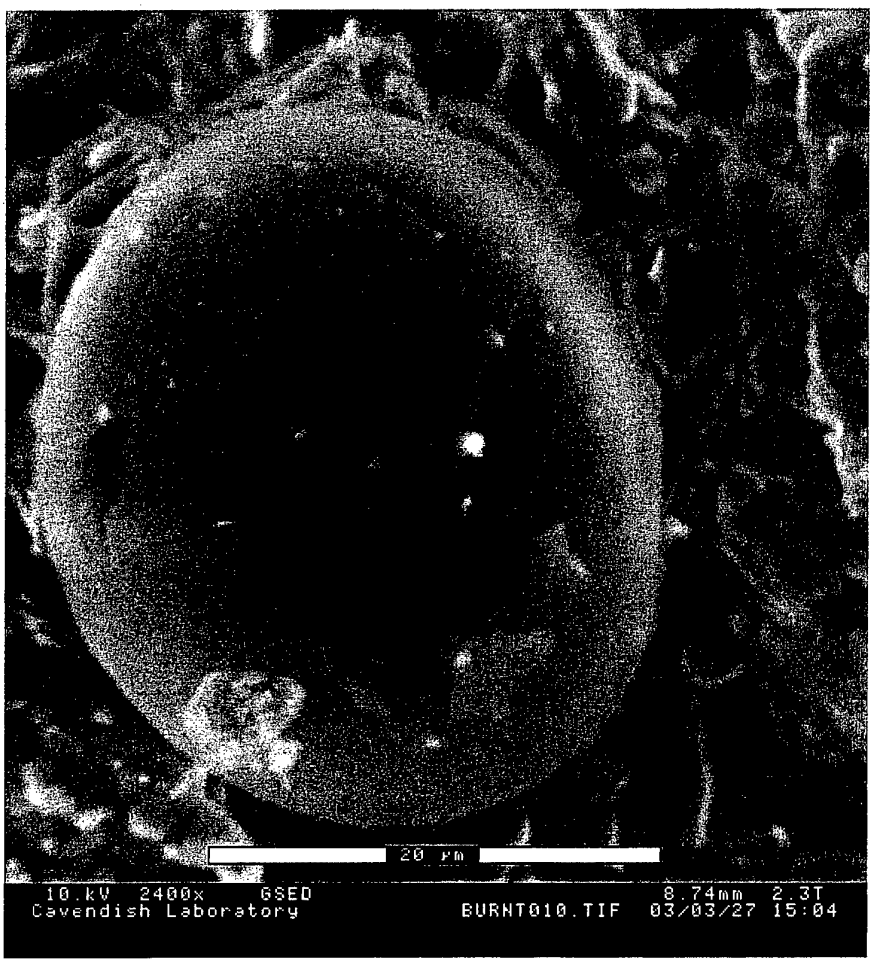

Figure 31. Fractured air bubble found in ignited sample, note the faint surface structure evident beneath the surface.

Figure 32. A second fractured bubble. Again structure is visible beneath the surface.

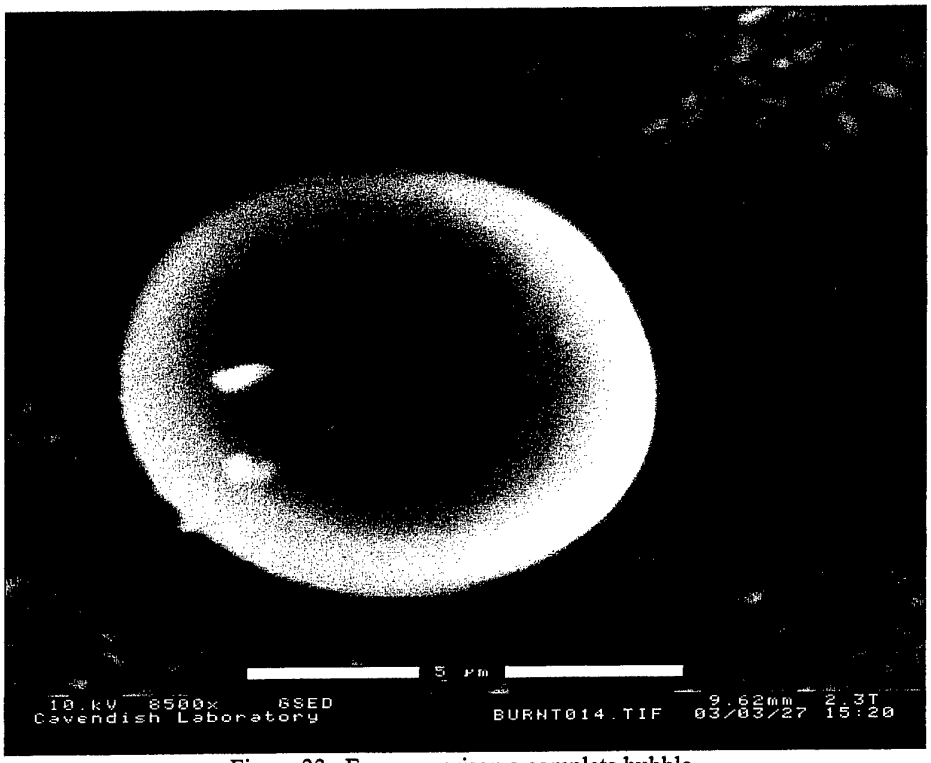

Figure 33. For comparison a complete bubble.

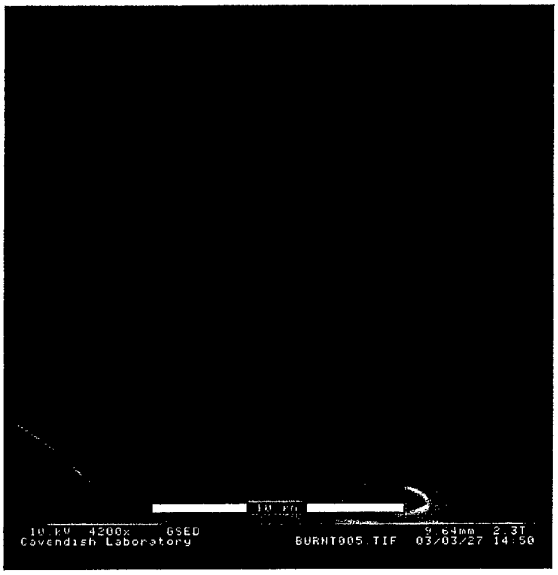

Figure 34. Melted crystals in the burnt sample.

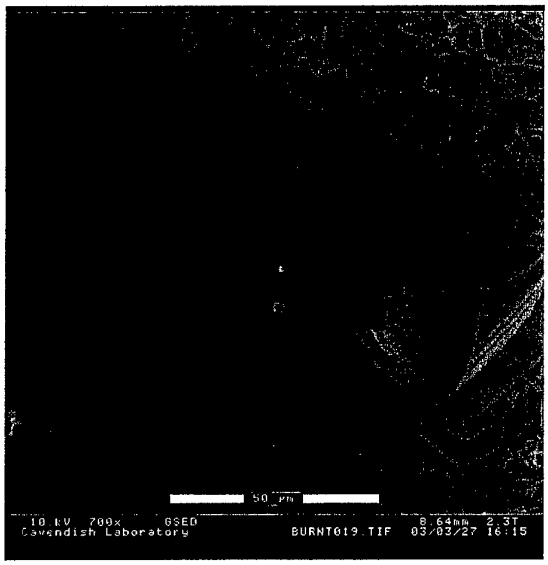

Figure 35. The type of crystals generally present.

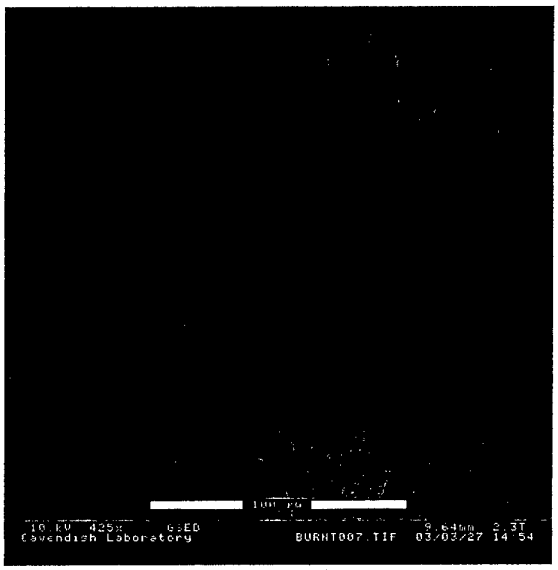

Figure 36. Fern-like growth structure present.

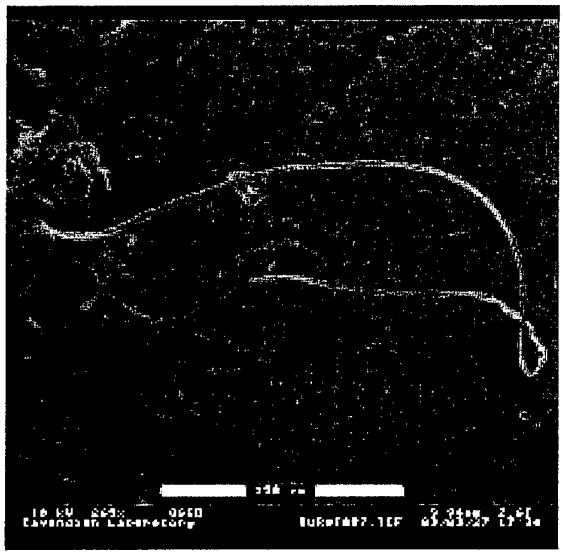

Figure 37. String-like structure present in the sample.

5.2 Quenched Samples

The liquid nitrogen quenched samples were inherently unstable and were prone to destruction under beam currents as low as 3 kV (Figure 38, i.e. significantly lower than the 10 kV used on the other samples. A wide variety of structures were found including a melted background matrix which consisted of a layer-like structure and several lamellar needle-like structures (Figures 39 and 40). These were highly regular with the middle of the structures tending to be around 2 microns in width (Figure 40), they were protruding from the melted background matrix but appeared to be a great deal more stable. These tended to be randomly distributed throughout the sample. Many of the ends were fissured suggesting that the growth had been rapidly stopped.

Growth tips could be seen in some areas indicating that growth begins at a nucleation site and may be due to some structure within the sample being drawn out at the onset of melting and the growth was instantly stopped by the rapid quench (Figure 41).

Large numbers of these needle-like structures and large crystals could be seen, similar to those seen in both the heated samples and those which had interacted with the plasma.

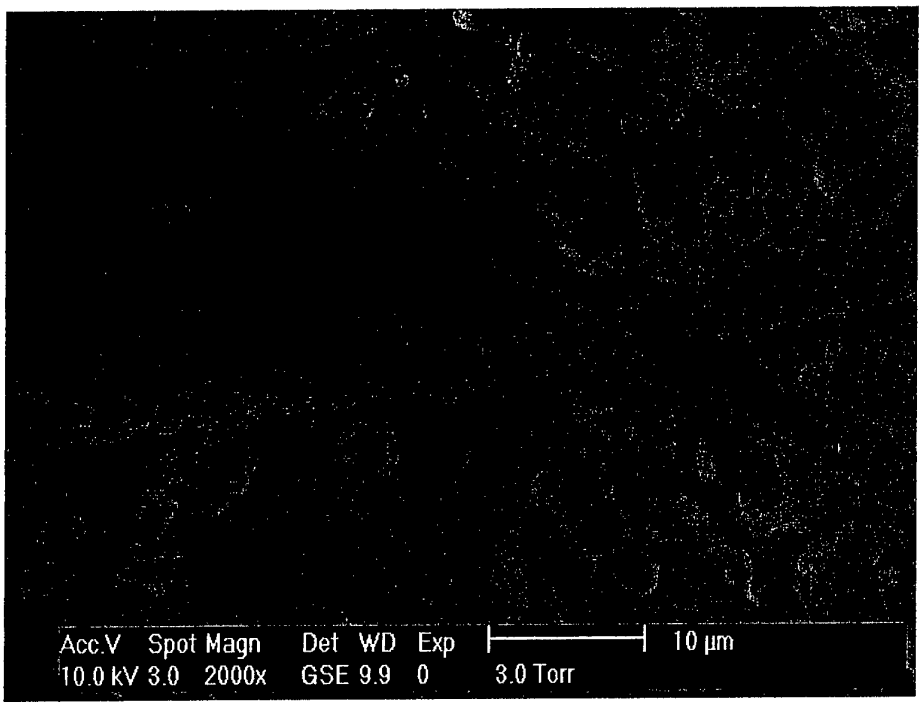

Figure 38. Evidence of the instability of the sample. The spherical features on the needles are where melting, leading to breakdown.

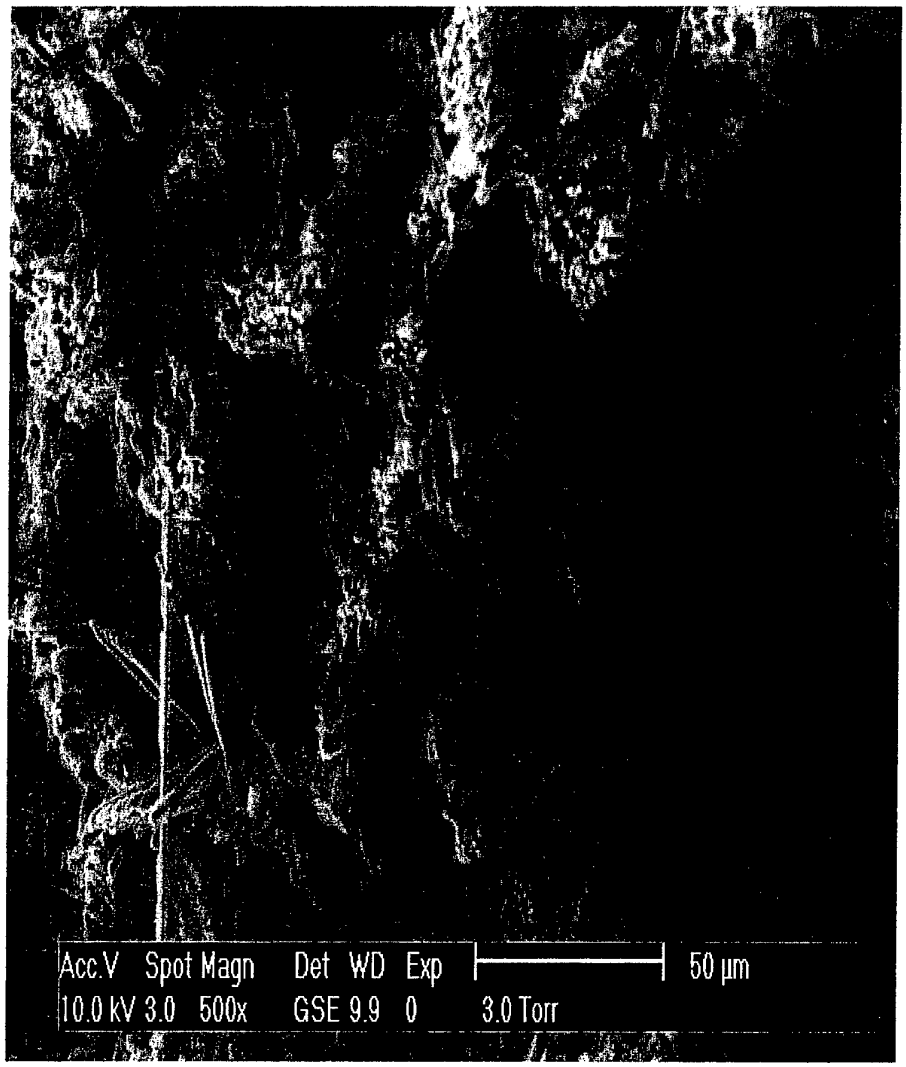

Figure 39. Needle-like structures to the left and right of the picture. Background matrix has the appearance of being a general melt structure. It is this back matrix which is the more unstable. Sample of RF69.

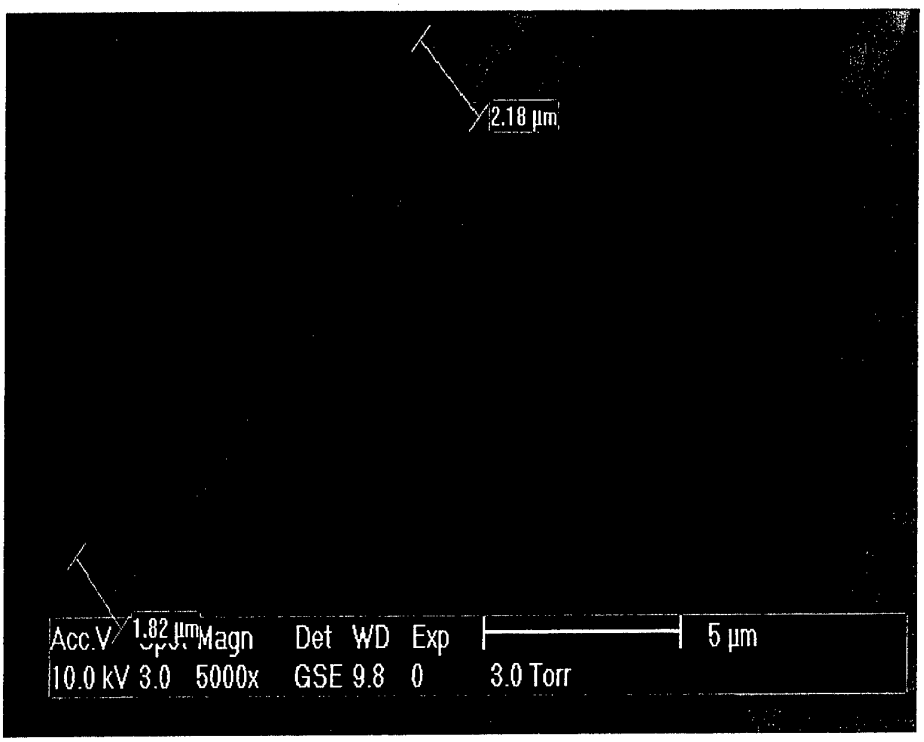

Figure 40. Close-up of the lamellar structures within the needles.

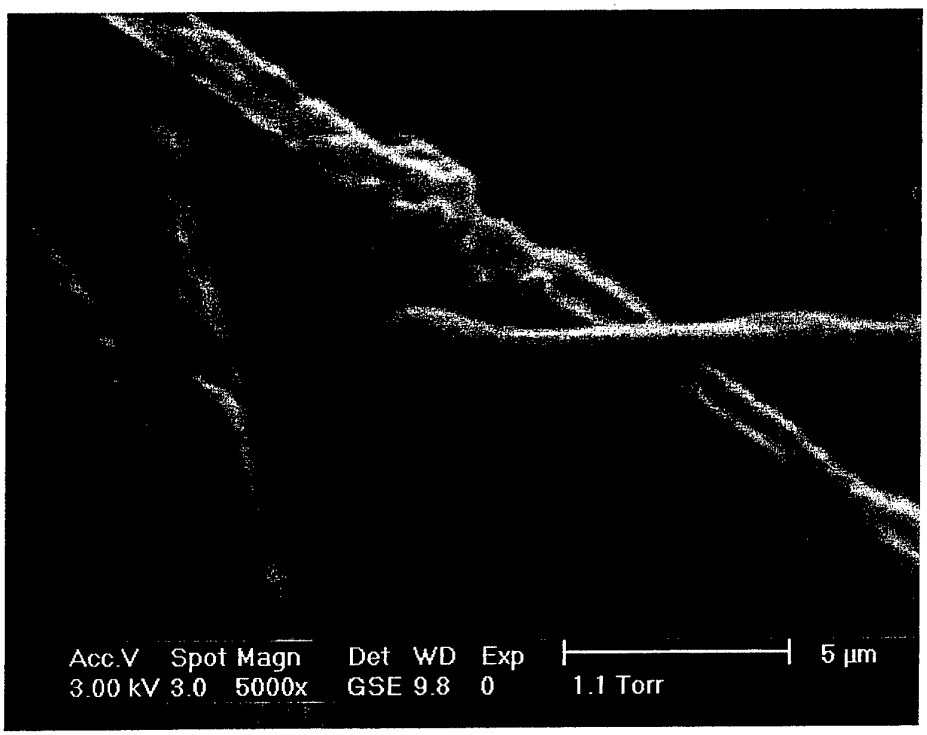

Figure 41. Needle growth tip just prior to destruction by the beam current.

6. Discussion

The four propellant samples and three methods of stimulating the propellant show a wide range of structures, varying degrees of stability and varying length-scales. A distinct ordering in stability was observed. This ran from most to least stable as (i) the burnt and fired samples, (ii) the fired samples and (iii) the liquid nitrogen quenched samples. Since (i) is the most stable it suggests that the burning uses the most active ingredients leaving relatively stable material. By simply firing the tungsten wire (ii) the propellant is only partially consumed. Finally, quenching a reacting sample (iii) leaves behind reactive structures, for example, high surface area material such as filaments and needles.

In the heated samples, large crystals were observed. These are present in undamaged samples but tend to be less abundant and much smaller. This appears to indicate that some kind of recrystallisation process is involved whereby perhaps the individual crystals seen in the undamaged sample aggregate to form the large crystals and the higher abundance is accounted for by recrystallisation of one of the components of the background matrix.

The droplets of tungsten observed were usually 2 to 5 μm in diameter though examples of up to ~30 μm were observed.

The images shown in Figure 42 were taken using high-speed photography at intervals of 2 μs and show that the spark starts at the two electrodes and spreads until the discharge from either side meet in the middle and cause the wire to explode. This may indicate a larger amount of material is spread out from the ends of the wire than the middle.

Figure 42. High-speed photographic images of an exploding wire. Frame interval 2 μs.

The bubble structures found in Figures 31-33 suggests that pockets of gas develop within the propellant expand upon heating causing the binder material to dome over them. The string-like structures found in Figure 37 could be a similar structure to the needles found in Figures 38-41 but with a change in morphology due to the heating.

The needle-like structures are likely to comprise of thin rods of binder material which have been drawn out by the initial heating and then rapidly truncated by the quenching process. The laminar structure suggests that as the material is drawn or flows outwards partial cooling occurs and a layer-like structure is built up in local regions. The extreme instability of this particular set of samples made them very difficult to work with and as such one should be wary of any artefacts which may have been added. This instability was a problem even at extremely low beam voltages with this particular damage occurring at 3.0 kV compared with the 7 to 10 kV beams used in earlier sections.

7. Deflagration to Detonation Studies

7.1 Introduction

The mechanism by which a deflagration makes the transition to a detonation is not yet fully understood. The salient features observed in the DDT of a granular secondary explosive are an accelerating combustion wave which moves through the unreacted charge, followed by the onset of detonation at some point down-stream from the combustion wave. A retonation wave can sometimes be seen to run upstream from the point of initiation. Central to this process is the formation of the shock waves which ultimately lead to detonation. This final shock-to-detonation transition is fairly well-understood; it is the mechanism by which sufficiently strong shock wave are first formed which is less clear. Early research on DDT is reviewed in McAfee et al. (1993) and Luebcke et al. (1995). Figure 43 gives schematically the DDT model proposed by McAfee et al. (1993).

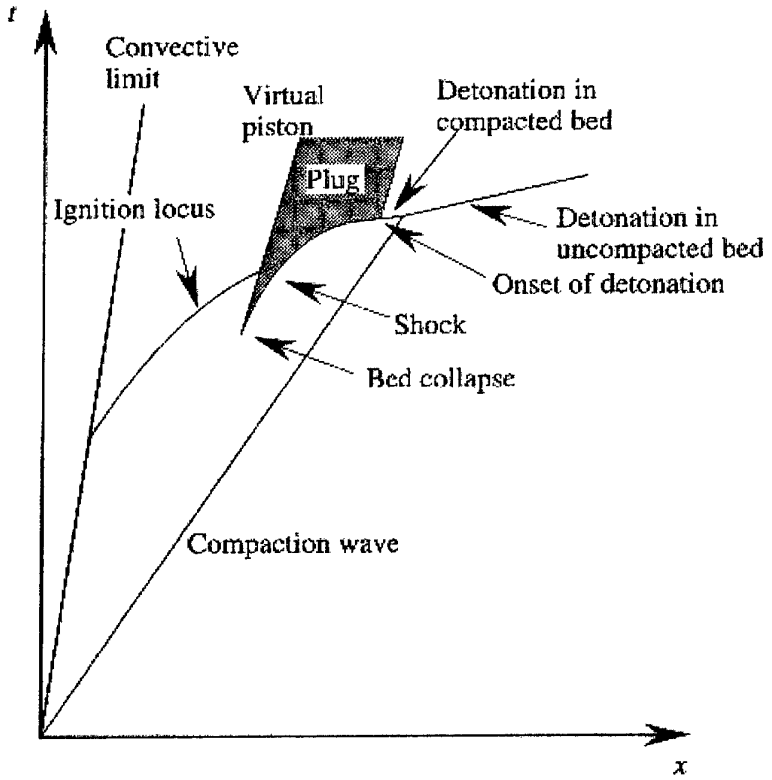

Figure 43. Graphical representation of the DDT model proposed by McAfee et al. (1993).

7.2 Experimental

The granulated explosives chosen for the Luebcke et al. study were 2-(5-cyanotetrazolato) pentammine cobalt (III) perchlorate (CP) and pentaerythritol tetranitrate (PETN). CP, a yellow free-flowing crystalline material with crystal density 1.97 g cm^{-3}, has been shown by Baer et al. (1986) and Stanton et al. (1981) to be highly reactive with growth to detonation occurring after only a few millimetres from the point of ignition. This may be due to it having a low shock initiation pressure. CP is thus ideally suited to small-scale laboratory investigation of DDT. Baer et al. (1986) reported the average particle diameter of their batch of CP, the same used in our study, to be of the order of 140 μm, but that under the action of pressing the particles easily fragment, resulting in an average particle size of 10-15 μm. The chemical structure of CP is more closely related to that of many inorganic primary explosives, such as mercuric-5-nitrotetrazole, than to most secondary explosives which are generally organic CHNO compounds.

High-speed photography was used to record the reaction of thermally ignited columns of CP and PETN. Thick walled metal confinement is normally used for DDT studies, which does not permit direct photographic study, although some workers (Demissy and Michot 1988; Dickson et al. 1991) have used fibre-optic probes to follow the reaction zone in beds of energetic material. The confining material chosen for CP was polycarbonate, which, although having a lower yield strength than metals, was found to be strong enough to permit DDT to occur in CP and thus gave the advantage of allowing direct visual observation of the reaction along the entire column length. However, polycarbonate does not provide sufficient confinement for PETN to undergo DDT. Therefore a steel confinement system fitted with a polycarbonate slit window was developed for PETN charges, which does allow direct and continuous high-speed streak photography.

Figure 44 shows the construction of the test-pieces. A fibre-optic probe was positioned at the ignition end of the explosive column so that light emitted from the initial stages of deflagration could be used to trigger the camera. The acceptance angle of the fibre-optic was reduced (to prevent premature triggering) by lengthening the fibre sleeving at the end of the fibre.

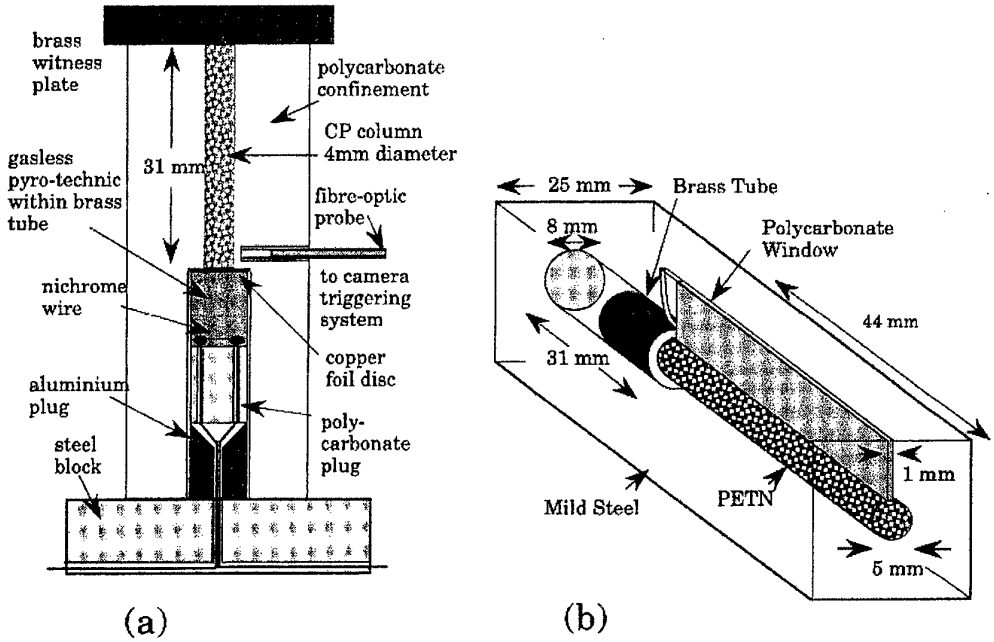

Figure 44. (a) CP and (b) PETN confining arrangements.

The charge was prepared by pressing the explosive incrementally, the height of each increment being less then the diameter of the explosive channel in order to ensure a consistent pressed density.

7.3 Results

The CP was examined by scanning electron microscopy to determine its particle size distribution. The particles, which ranged in sized from 20 to 200 μm, appeared to consist of loosely bonded clusters of smaller octahedral crystals in the range 2-30 μm. Examination of pressed samples showed that these clusters usually disintegrate during the pressing process.

The high-speed streak photographs of the progress of the reaction front through CP and PETN were scanned and digitised to facilitate accurate measurement of deflagration and detonation velocities and run-to-detonation lengths. The digitised records of the position of the reaction front with time were also differentiated to give velocity-time profiles.

Figure 45 is a plot of run-to-detonation length against %TMD, which indicates that this rises with pressed density up to the point at which it exceeds the length of the columns used in these tests. The errors in the density and run-to-detonation length were estimated to be 6% and 1 mm respectively. It differs from the commonly observed 'U-shaped' plots of many other secondary explosives in that there is no evidence of the run-to-detonation length increasing at lower densities. Run-to-detonation lengths for the stepped density columns were not significantly different to those for uniform pressings, indicating that shock wave formation at density discontinuities have little effect on the DDT process in this situation.

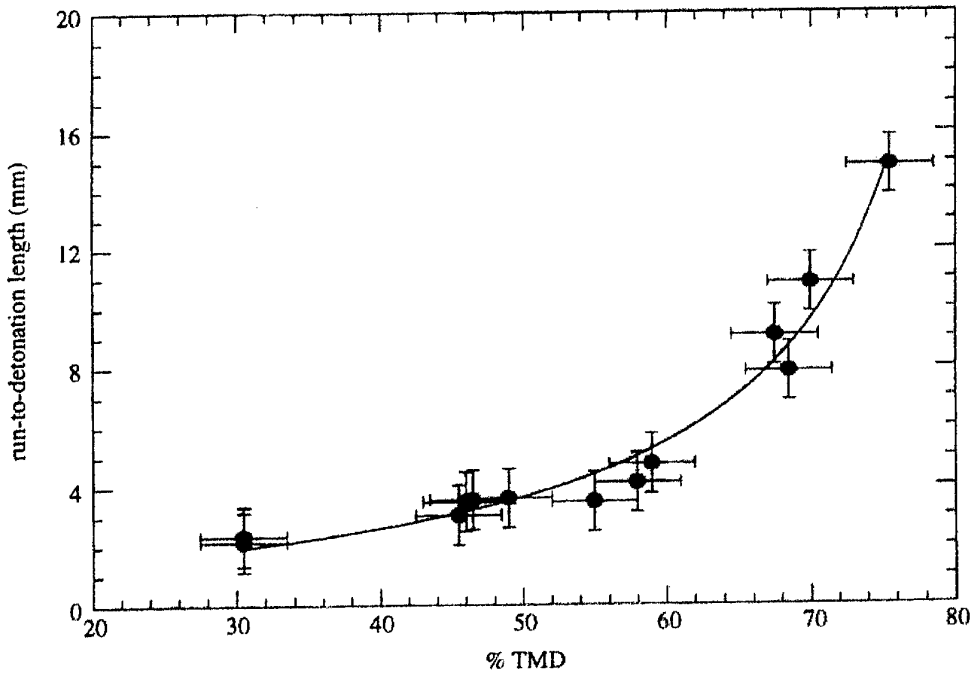

Figure 45. Run-to-detonation length versus %TMD for CP

Figure 46 shows DDT in a column pressed to 67% TMD which exhibits a run-to-detonation length of 12mm and an accelerating deflagration which increases to 1.5 mm μs^{-1} immediately before DDT. In a column pressed to 58% TMD there is a 6 mm run-to-detonation length and an apparently constant deflagration velocity of 1.1 mm μs^{-1} which increases to 1.5 mm μs^{-1} immediately before DDT.

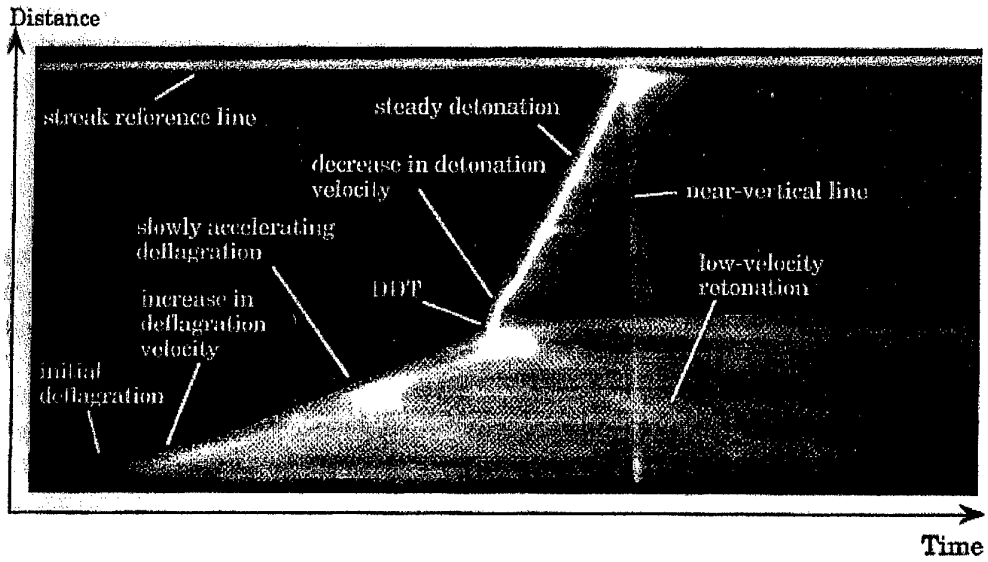

Figure 46. Streak record of DDT in 67% TMD CP.

At DDT, the change in velocity appears to be discontinuous, with an initial detonation velocity of 6.0 to 6.5 mm μs^{-1} which is maintained for 2 to 3 mm, before decreasing to a stable value of 5.5 to 6.0 mm μs^{-1}. A low velocity shock wave is visible moving upstream from the point of DDT at a velocity of about 1.7 mm μs^{-1}. This velocity does not appear to depend on either the velocity of the preceding deflagration or the subsequent detonation.

Occasionally a near-vertical line appears on the streak record (labelled in Figure 46) at the time when the detonation reaches the witness plate. This is thought to be due to adiabatic compression of the small air-space at the end of the column causing light emission which is then scattered by the decomposition products throughout the column.

7.4 Ultrafine Explosives DDT (type I) and DDT (type II)

Type II DDT was observed in charges of picric acid in Russia (Ermolaev et al., 1988; Khrapovskii, 1993 and Khrapovskii and Sulimov, 1995) and tetryl (Bernecker and Price, 1976) and some high-energy propellants in the US (Price and Bernecker, 1981). All of the charges in which this mechanism was displayed had a high porosity (<50% theoretical maximum density) and a small particle size (<20 μm).

More recently type II DDT has been observed by us in charges of PETN and RDX. The mechanism operates in low density charges made using ultrafine (<1 μm primary particle size) powders.

7.5 Ultrafine PETN

Experiments carried out on columns of ultrafine PETN pressed to densities greater than 50% TMD showed that the columns would either undergo a type I DDT or not make the transition to detonation at all and simply deflagrate. A typical streak photograph of type I DDT event in a column of ultrafine PETN is shown in Figure 47. The major features of the event are as those for the columns of conventional grain PETN described above. In Figure 47 it can be seen that at 'A' there is a double front proceeding along the column. It is thought that the slower of these corresponds to a convective burning stage proceeding behind the compressive front; the earlier conductive burn having occurred prior to the camera being triggered in the first few millimetres of the PETN column. The velocity of the convective burning is 0.15 ± 0.01 mm μs^{-1}. At 'B' the convective burning front catches up with the point at which the compressive burning began. The velocity of the burning immediately after the onset of compressive burning began at 'A' can be measured and is 0.49 ± 0.02 mm μs^{-1}. As can be seen from the photograph, the compressive burning accelerates smoothly except for a sudden increase at 'C'. Just prior to the plug reaching the critical velocity and pressure required for a shock initiation to occur, the compressive wave is propagating along the column at 0.93 ± 0.03 mm μs^{-1}.

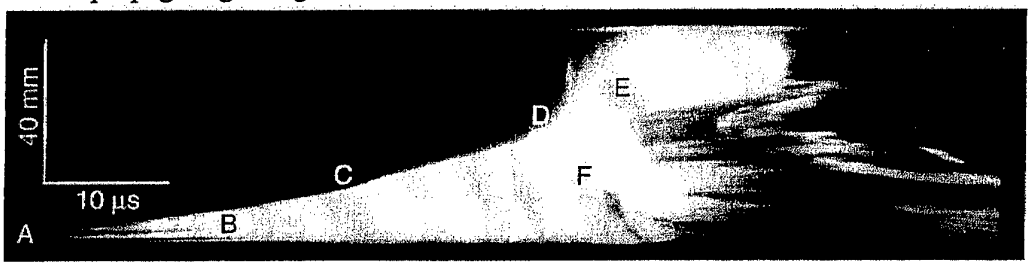

Figure 47. A type I DDT event in ultrafine PETN.

The transition to detonation occurs at 'D' the downstream face of the unreacted plug. The detonation wave (E) then proceeds along the remainder of the column at a steady velocity of 3.6 ± 0.2 mm μs^{-1}. Also emanating from the point at which the detonation breaks out is a retonation wave (F). This travels back through the unreacted plug and the partially reacted material behind it at a velocity of 5.0 ± 0.2 mm μs^{-1}.

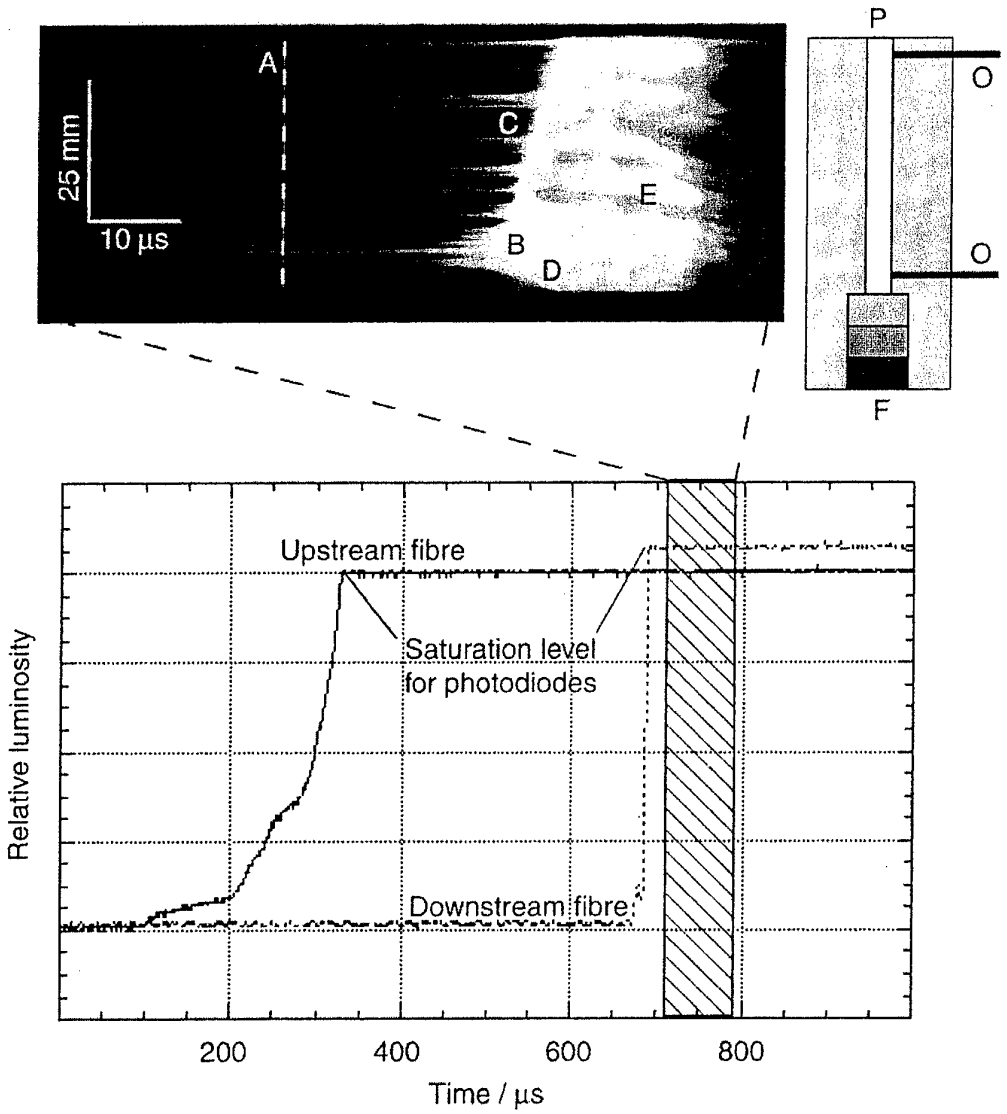

Figure 48. Streak photography of a type II DDT event in ultrafine PETN. A schematic of the column configuration is shown to scale to the right of the photograph. The output from the photodiodes is shown below. The shaded region of the graph corresponds to the period covered by the streak record. P – PETN column; O- optical fibres; F – Fuse.

Figure 48 shows a streak record of type II DDT process occurring in a charge of ultrafine PETN pressed to a density of 29 ± 1% TMD. A schematic of the confinement is shown next to the streak record at the same scale as the photograph. The graph below the streak record is a record of the luminosity at the two optical fibres. As can be seen, the initial convective burning stage takes some 600 µs to propagate along the length of the column. The column then continues to burn for a period of around 70 µs before the detonation breaks out. The streak record (running during the period indicated by the hatched area on the graph) gives detail of the events in the final 40 µs prior to the detonation and the following 30 µs.

At the time indicated by the dashed line 'A', it can clearly be seen that reaction is taking place at a number of points which appear stationary on the time scale of the streak record. As the camera can only image the surface of the column it can be surmised that these reaction sites are in the part of the charge in contact with the window. The luminosity of the reaction at these sites continues to increase until at

site 'B' the conditions reach the critical parameters for initiation. There appears to be no shock wave associated with the build up to the initiation event. A detonation wave (C) then propagates downstream (relative to the ignition site) at an average velocity of 5.4 ± 0.2 mm μs^{-1}. There is also an upstream retonation wave (D), that propagates from the point 'B', but the proximity of the initiation to the upstream end of the column makes any calculation of the velocity of this wave difficult.

A reflected shock (E) travelling at 2.23 ± 0.09 mm μs^{-1} can also be seen propagating upstream from the point at which the detonation (C) reached the witness plate at the downstream end of the column.

Other experiments have shown that the position at which the initiation takes place is not fixed. Figure 49 shows a streak record from a confinement pressed to the same density as that in Figure 48. In this case initiation (A) took place near the downstream end of the confinement. The retonation wave (B) which propagated upstream from the initiation point is travelling upstream at an average velocity of 5.6 ± 0.3 mm μs^{-1} although as can be seen from the record this velocity is not constant.

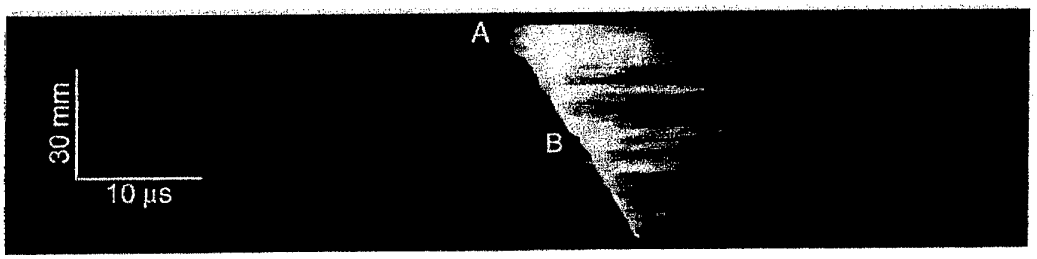

Figure 49. Type II DDT event in ultrafine PETN.

The experiments in which type II occur are all similar in the way in which the reaction proceeds, but the point at which the detonation breaks out can be anywhere along the length of the column. The first step appears to be the formation of a channel in the low density material during the convective burn stage. There appears to be no correlation between either column length or density and the position of the detonation break-out.

7.6 Ultrafine RDX

The results from the experiments carried out on ultrafine RDX closely resemble those described above for ultrafine PETN. As with the PETN it was found that dense columns (in the case of RDX this was over 50% TMD) did not undergo a DDT transition of either type in the lengths of column used in this study. A streak record of a deflagrating charge of ultrafine RDX pressed to $61 \pm 1\%$ TMD is shown in Figure 50. The record shows the compressive burning as it propagates along the column. The luminosity of the deflagration varies as it proceeds through the charge. The velocity of the front is fairly constant at around 0.62 mm μs^{-1} for the duration of the streak record.

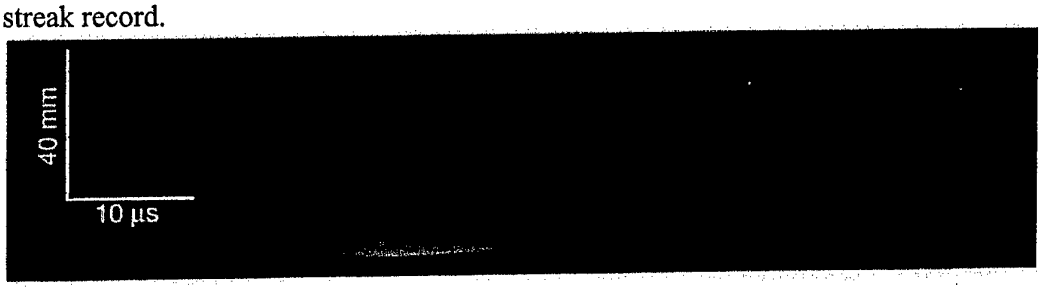

Figure 50. Streak record of a deflagrating charge of ultrafine RDX.

Columns pressed to below 50% TMD underwent a type II DDT. This has all the major features of the type II DDT as described for PETN. The streak record in Figure 51 shows a typical event in a column of ultrafine RDX pressed to 37% TMD. As with the PETN, a conductive burning stage rapidly gives way to a convective burn as product gases are given off during reaction. This proceeds to the end of the column. The luminous regions in the streak record (A) do not appear to be as stationary as they were in the PETN charges. This is due to pressure and release waves reflecting along the column and carrying with them the material or gas that is causing the light emission. The detonation waves break out at 'B' and then travel along the column in both directions at slightly different speeds. The wave travelling downstream 'C' propagates at 2.1 ± 0.3 mm μs^{-1} whilst the upstream wave travels at 'D' 1.8 ± 0.3 mm μs^{-1}.

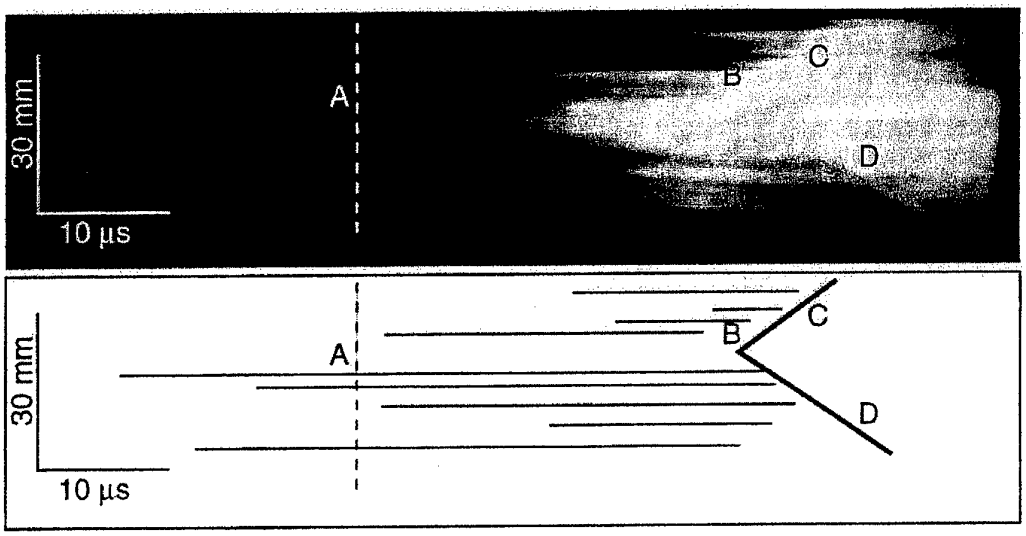

Figure 51. Steak record of a type II DDT event in a column of ultrafine RDX. A schematic of the photograph is given for clarity.

No type I DDT events were observed in columns of ultrafine RDX during this study.

7.7 Conventional RDX

The charges of conventional RDX either deflagrated when they were at a density above 75% TMD or underwent a type I DDT when the density was below this level. In none of the experiments involving conventional RDX was a type II DDT observed.

Figure 52 is an example of a type I DDT occurring in a charge of conventional RDX pressed to a density of 70 ± 1% TMD. As with the other type I DDT events described above the event shown in Figure 52 passes through a conductive and convective stage before the compressive burning starts at 'A'. The compressive burning is initially at a low luminosity. After becoming visible (B) in this record it is propagating at 0.90 ± 0.1 mm μs^{-1}. The plug being pushed ahead of the reaction front finally reaches the critical pressure required for a SDT event at 'C' causing a detonation (D) to propagate along the remainder of the column. The detonation propagates at 8.2 ± 0.2 mm μs^{-1}. A rearward travelling high luminosity shock can also be seen propagating at a velocity of 2.0 ± 0.2 mm μs^{-1}.

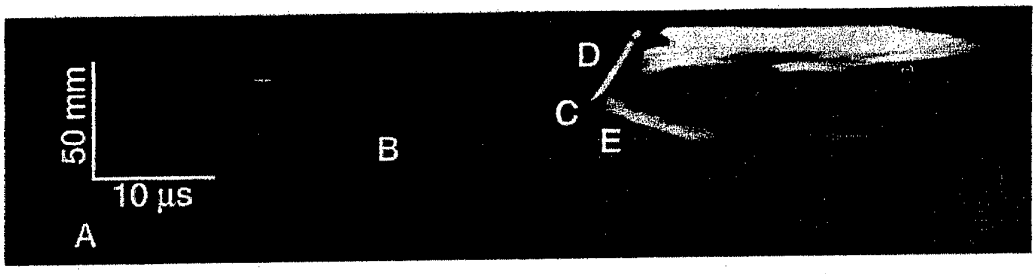

Figure 52. A streak record of a type I DDT event in a charge of conventional RDX.

7.8 Post-Mortem Results

Post-mortem examination of the confinements shows a marked difference between the deflagration events, the type I and type II DDT events. Figure 43 shows three copper cylinders which are typical of the three different types of event.

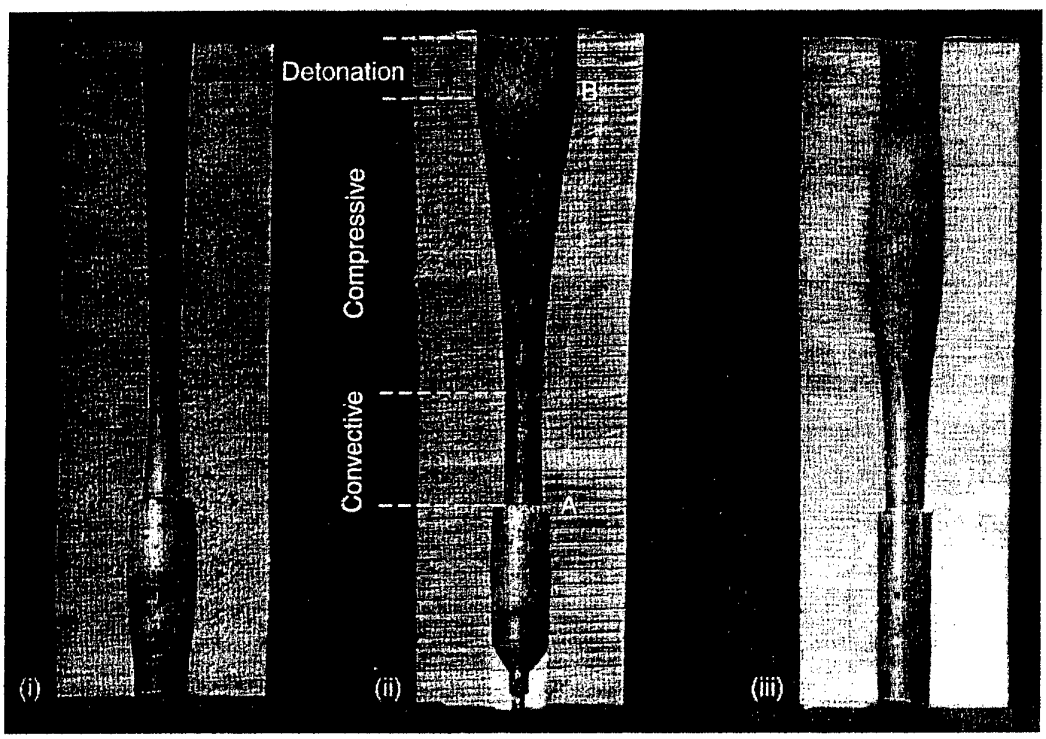

Figure 53. Examples of copper cylinders for post-mortem examination. (i) Deflagrating charge; (ii) Type I DDT; (iii) Type II DDT.

Cylinder (i) was originally packed to a density of 60 ± 1% TMD with ultrafine RDX. The charge underwent a deflagration event. As can be seen the channel in which the charge was laid has suffered very little distortion and the surface of the channel is unmarked.

Cylinder (ii) was originally packed to a density of 75 ± 1% TMD with conventional RDX. This confinement is typical of a cylinder in which a type I DDT event has taken place. After ignition at 'A' the reaction has progressed as a convective burn for approximately 17 mm along the column. In this region the channel surface has suffered very little marking. When the deflagration has moved into the compressive mode, the high pressures cause far more distortion to the column that the convective deflagration did. As can be seen the channel is widened by the pressures and reaches a maximum width at 'B', 62 mm along the column. This corresponds to the point at which the plug of compressed material reaches the critical density and velocity

required to initiate the column. Detonation occurs at the downstream face of the plug and proceeds along the remainder of the column. The channel walls in the detonating region have characteristic striations and the channel width in this region is fairly constant.

Cylinder (iii) was packed to a density of 40 ± 1% TMD with ultrafine RDX. A type II DDT event has occurred in this column. It is difficult to say precisely where the detonation broke out within the column, but it can be seen that the distortion to the internal surface of the column is severe when compared with that of column (i); despite the lower density of the material in the column originally. As has been seen in the streak records above, this type of event lacks the obvious directionality of the type I DDT event with detonation and retonation appearing very similar on the picture. This is born out by the post-mortem examinations in which no obvious direction can be found except for the low level of distortion near the initial ignition point.

7.9 Key Points

The key points that have arisen from the study described in this chapter are as follows.

- Type II DDT has been observed in low density charges of ultrafine PETN and RDX. It appears that during the convective burn stage a channel is created in the charge.
- The velocity of detonation following type II events is greater than expected for PETN.
- The run-to-detonation distance for type I events in PETN is usually longer for ultrafine material than conventional material.
- There appears to be no compressive deflagration during the type II DDT events.

8. Gas permeation through granular beds

This part of the overall project is concerned with the response of granular beds to high pressure, short duration gas pulses. We are interested in studying the propagation of combustion gases, including plasmas, through compacted beds of inert or explosive material. The experimental results should aid understanding and modelling of plasma ignition and the deflagration to detonation transition (DDT).

The experiment utilises a gas gun, high-speed speckle photography and fast pressure response gauges. High-speed photography will give us information on the movement and behaviour of particles within the bed. Pressure measurements will enable us to determine energy losses and complex properties such as viscous drag.

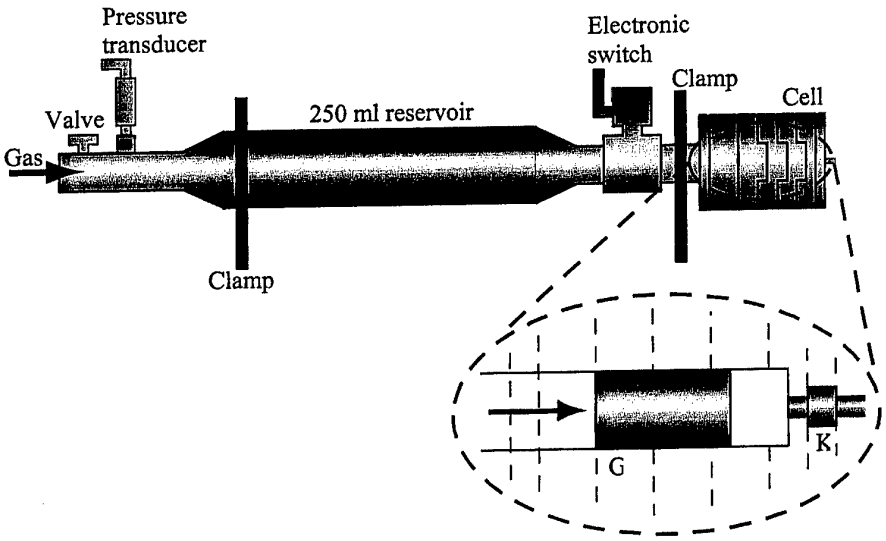

Figure 54. Schematic of the equipment for gas permeation studies.

Figure 54 gives a schematic of the apparatus. The valve and pressure transducer are used to fill the reservoir to a known pressure (up to 100 bar). An electronic switch is used to "open" the reservoir and allow gas to flow into the cell until pressure equilibrium is reached. A diaphragm can be added after the electronic switch to provide an even sharper pressure release. Alternatively a plasma discharge can be created by depositing electrical energy into a thin wire.

The cell is constructed of multiple flanges which slot together. The sample of granular material is pressed directly into the flanges and by altering the number of flanges bolted together in the cell, we control the sample length. A high-speed Kistler pressure transducer (K) is used to measure the pressure-time history of the gas permeating through the granular bed (G).

Investigations into the profile of the gas pulse produced by this system have been conducted. The traces below show pressure-time histories recorded by the pressure transducer when gas is released into the cell. Two different methods for releasing the gas have been compared to date.

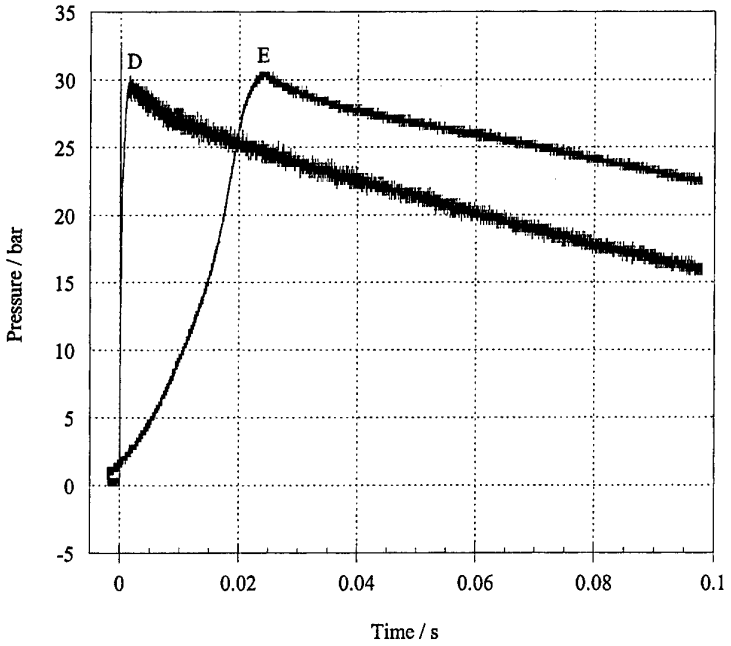

Figure 55. Pressure versus time traces.

The trace labelled E in Figure 55 was obtained by pressurising the reservoir with 40 bars of nitrogen and releasing using only an electronic valve. A shorter rise time was achieved by introducing a bursting diaphragm after the switch. The diaphragm consists of a small sheet of metal shim clamped between the first two sections of the cell. The metal shim fails and allows gas propagation into the cell if the pressure is sufficient. The larger pressure gradient produced in this case (trace D) is a better simulation of the gas front recorded in enclosed combustion experiments.

The chosen diaphragm material and thickness determine the bursting pressure and the peak pressure recorded by the pressure transducer. We have studied numerous materials to cover a range of pressures. Some example results are shown below; here we have investigated 0.002" and 0.004" thick aluminium, 0.001" and 0.002" brass, 0.002" phosphor bronze and 0.0025" beryllium copper. Solid markers represent experiments where the diaphragm burst and hollowed markers represents diaphragms that did not burst.

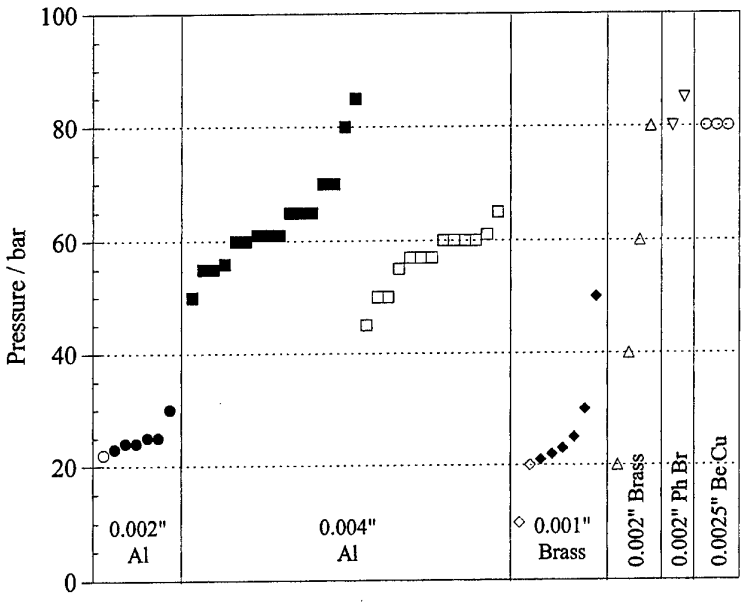

Figure 56. Pressures at which various diaphragm materials burst (solid markers) versus pressured for no burst for various materials (open markers).

It is the aim of these experiments to measure the losses as gas fronts, or plasmas, propagate through granular beds. Furthermore, optical techniques will be utilised to monitor the behaviour and movement of particles within the bed under the influence of these high pressure gases pulses. These techniques such as high-speed photography and experience in monitoring movement using digital speckle algorithms are available in the laboratory.

9. References

Baer, M R, Gross, R J, Nunziato, J W and Igel, E A (1986) An experimental and theoretical study of deflagration to detonation transition (DDT) in the granular explosive, *CP Combust. Flame* **65**, 15-30.

Bernecker, R R and Price, D (1976) Deflagration to detonation transition behaviour of tetryl, *Proc. Sixth Symposium (Int) on Detonation*, D J Edwards, Arlington, Virginia, Office of Naval Research, 426-435.

Danilatos, G D (1993) Introduction to the ESEM instrument, *Microsc. Res. Tech.*, **25** 354-361.

Demissy, M and Michot, C (1988) Fibre-optical probe detection in explosions: signal analysis, *Proc. 13th Int. Pyrotech. Seminar*, 163-171.

Dickson, P M, Field, J E and Luebcke, P E (1991) Experimental investigation into deflagration to detonation transition in secondary explosives, *Cavendish Report*, Cavendish Laboratory, Cambridge.

Ermolaev, B S, Sulimov, A A, Okunev, V A and Khrapovskii, V E (1988) Mechanism for transition of porous explosive system combustion into detonation, *Combust. Explosion Shock Waves*, **24** 65-68.

Farley, A N and Shah, J S (1991) High-pressure scanning electron microscopy of insulating materials: a new approach, *J. Microsc.*, **164** 107-126.

Khrapovskii, V E (1993) Initial stage of ignition process in powder explosive with a closed end, *Combust. Explosion Shock Waves*, **29** 129-134.

Khrapovskii, V E and Sulimov, A A (1995) Onset of convective burning in picric acid, *Combust. Explosion Shock Waves,* **31** 23-29.

Luebcke, P E, Dickson, P M and Field, J E (1995) An experimental study of the deflagration-to-detonation transition, *Proc. R. Soc. Lond. A* **448** 439-48.

McAfee, J M, Asay, B W and Bdzil, J B (1993) Deflagration-to-detonation in granular HMX: ignition, kinetics and shock formation, *Tenth Symp. (Int.) on Detonation*, Boston, MA: US Government Printing Office.

Price, D and Bernecker, R R (1981) DDT behaviour of porous columns of simple propellant models and commercial propellants, *Combust. Flame* **42** 307-319.

Rae, P J, Goldrein, H T, Palmer, S J P, Field, J E and Lewis, A L (2002) Quasi-static studies of the deformation and failure of β-HMX based polymer bonded explosives, *Proc. R. Soc. Lond. A* **458** 743-762.

Stanton, P L, Igel, E A, Lee, L M, Mohler, J M and West, G T (1981) Characterisation of the DDT explosive, CP, *Seventh Symp. (Int.) on Detonation,* Annapolis, MD: US Government Printing Office.

Stokes, D J, Thiel, B L and Donald, A M (1998) Direct observation of water-oil emulsion systems in the liquid state by environmental scanning electron microscopy, *Langmuir* **14** 4402-4408.

Thiel, B L, Bache, I C, Fletcher, A L, Meredith, P and Donald, A M (1997) An improved model for gaseous amplification in the environmental SEM, *J. Microsc.* **187** 143-157.

Acknowledgements

We are most grateful for the support on this contract. Monetary constraints curtailed the research described in Section 8. However, it is hoped to obtain new funding to complete these experiments.

Appendix A
Figures showing some of the equipment.

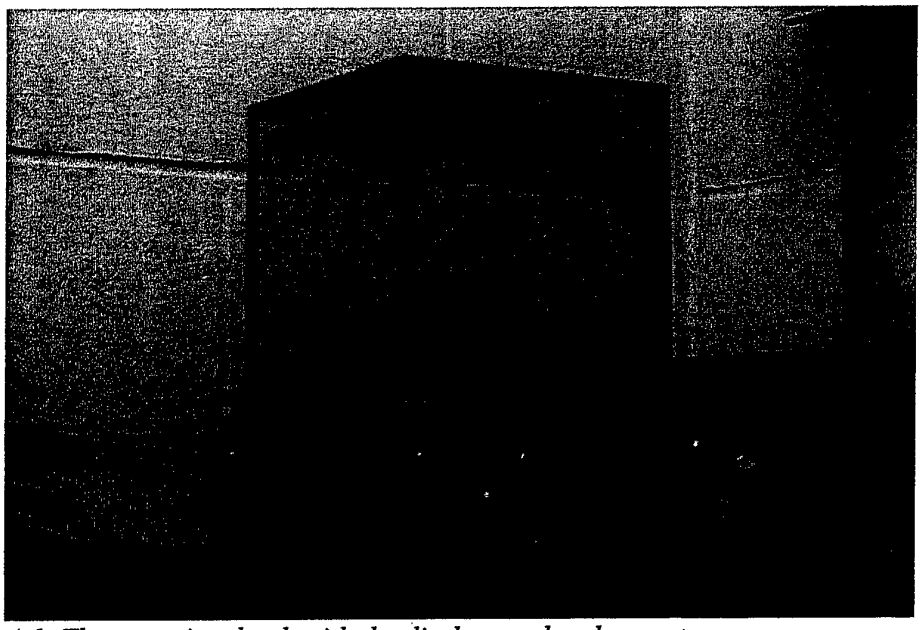

A 1. The capacitor bank with the discharge chamber on top

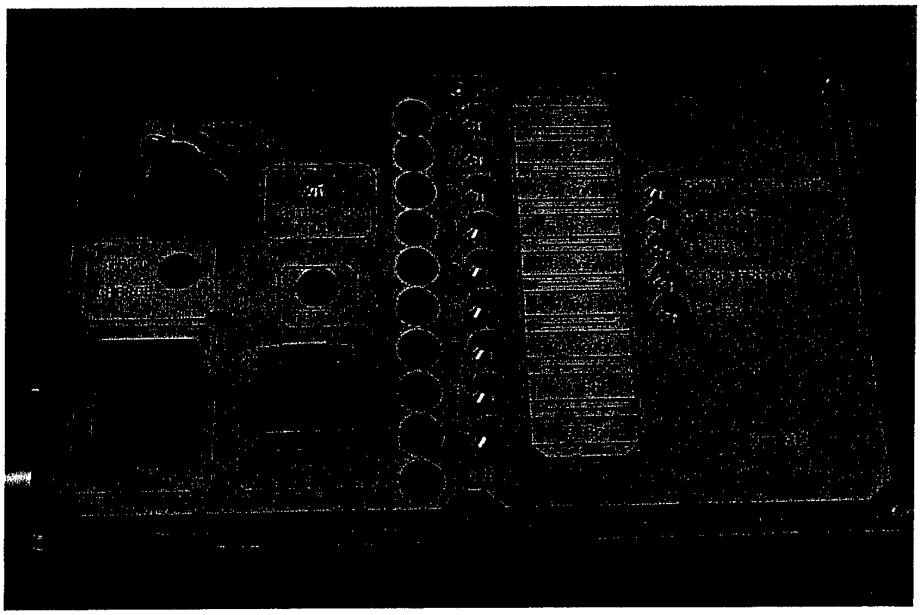

A 2. The control panel

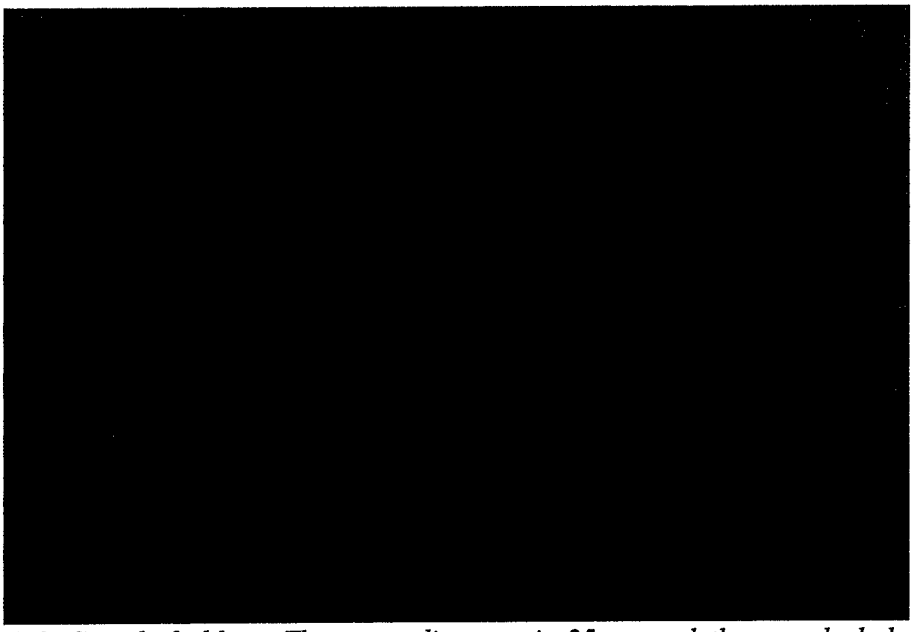

A 3. Sample holder. The outer diameter is 25mm and the sample hole is 2.8mm diameter.

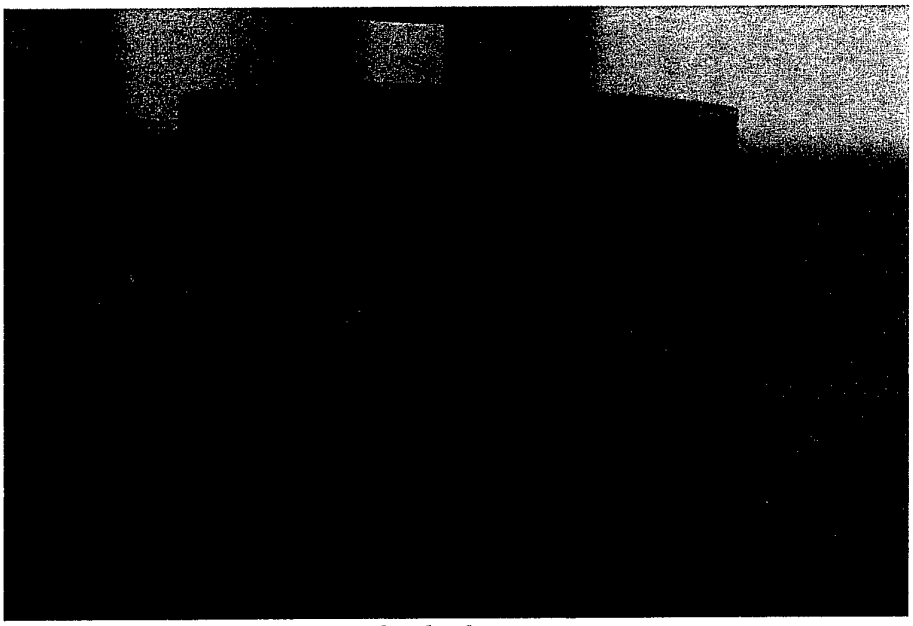

A 4. Sample holder in position for discharge

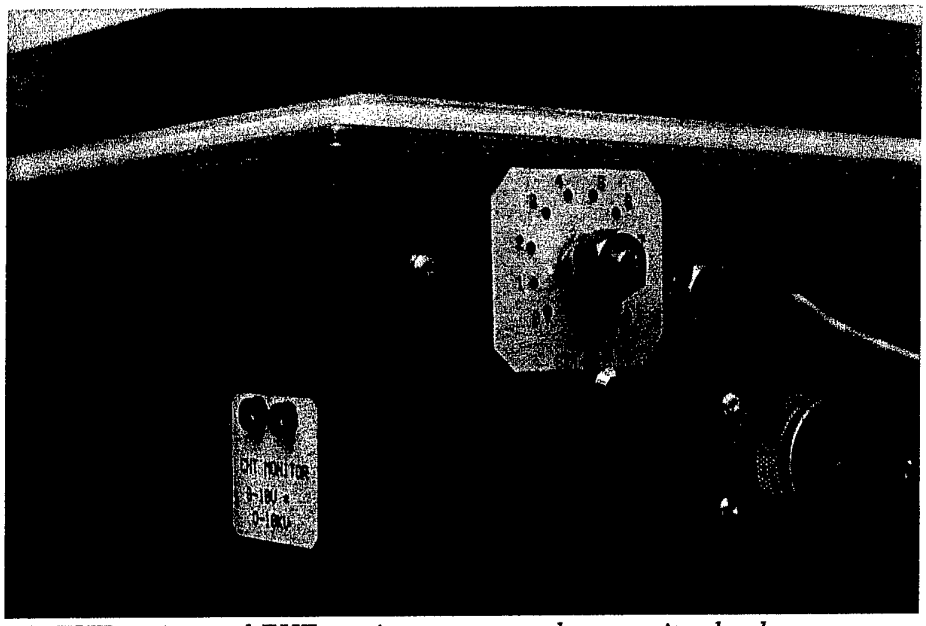

A5. EHT setting and EHT monitor output on the capacitor bank

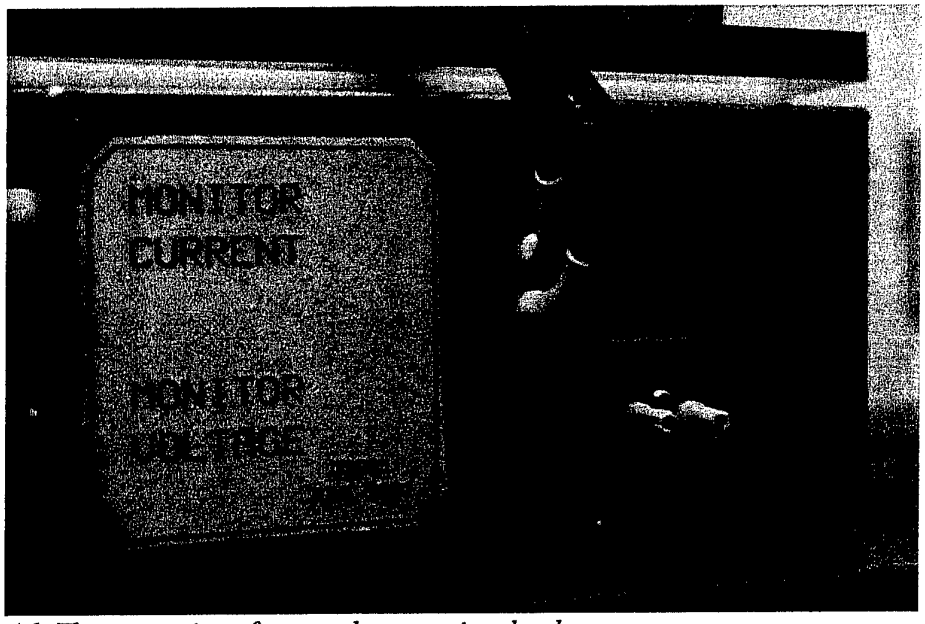

A6. The output interface on the capacitor bank

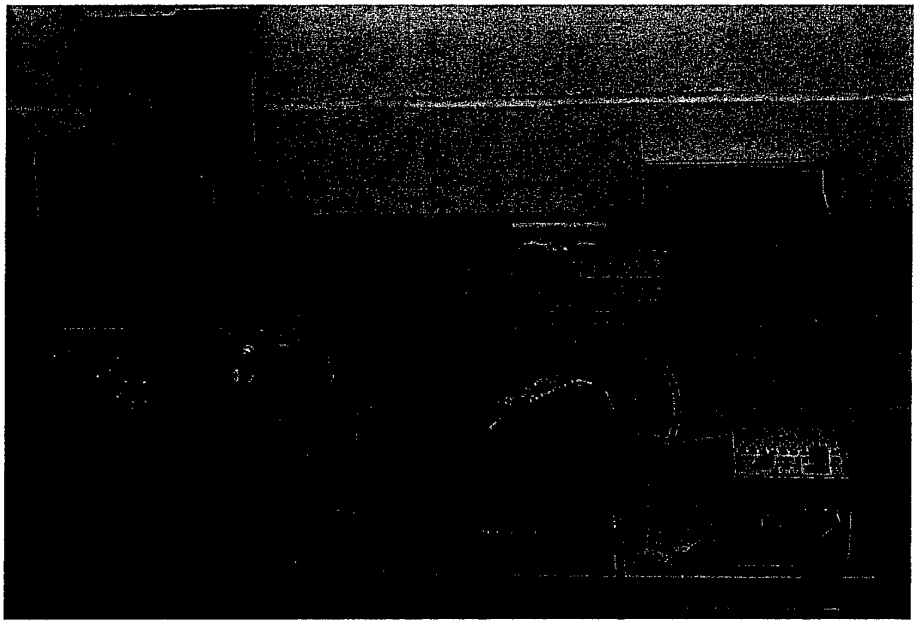

A7. The set-up configuration with one oscilloscope